DIPLOMARBEIT

Towards Uncovering the Charge Carriers in Tribocharging

ZUR ERLANGUNG DES AKADEMISCHEN GRADES

DIPLOM-INGENIEUR

IM RAHMEN DES STUDIUMS

TECHNISCHE PHYSIK

EINGEREICHT VON

MARKUS FELBER

MATRIKELNUMMER 11708441

supervised by

Ass. Prof. Dipl.-Ing. Dr.techn. Scott Waitukaitis, ISTA

Univ. Prof. Dipl.-Ing. Dr.techn. Markus Valtiner, TU Wien

May 2, 2024

Unterschrift Student

Abstract Deutsch

Wenn sich zwei elektrisch neutrale Objekte berühren, kann dies zu einem Ladungsaustausch führen. Dieses Phänomen nennt sich triboelektrischer Effekt oder "tribocharging". Obwohl dieser Prozess bereits seit über 2000 Jahren bekannt ist, sind viele Aspekte davon bis heute zu großen Teilen ungeklärt. Allen voran ist hierbei die Frage nach der Identität der Ladungsträger, welche für den Ladungsaustausch verantwortlich sind. Während oftmals Elektronen als wahrscheinlichste Ladungsträger gehandhabt werden, gibt es auch Thesen, in welchen Ionen für den Ladungstransport verantwortlich gemacht werden, da für beide Ansätze unterstützende experimentelle Ergebnisse vorliegen. Im Zuge dieser Arbeit wird deshalb ein Experiment entworfen, welches in weiterer Folge zum Ziel hat die Rolle von Ionen im triboelektrischen Effekt endgültig zu bestimmen. Dadurch, dass Ionen und Elektronen einen großen Massenunterschied aufweisen, wird ein Massenspektrometer verwendet. Die Idee des Experiments lautet wie folgt: Der triboelektrische Effekt wird verwendet, um zwei nichtleitende Proben aneinander elektrisch aufzuladen, danach wird eine der Proben nahe am Eingang eines Massenspektrometers erhitzt. Dieser Temperaturanstieg könnte zu Desorption von Ionen führen. Wenn die Anzahl der desorbierten Ionen mit der Gesamtladung der Probe korreliert, wäre die Existenz von ionischen Ladungsträgern im triboelektrischen Effekt unbestritten.

Um aber dieses Experiment umsetzen zu können, müssen zuerst einige grundsätzliche Fragen geklärt werden, was schlussendlich den Inhalt dieser Diplomarbeit darstellt. Abgesehen vom generellen Aufbau des Experiments ist ein essenzieller Punkt die Notwendigkeit eines passenden Ladungsmessungsapparats, da Objekte vermessen werden müssen, ohne jemals mit ihnen in Kontakt zu kommen. Dafür wird ein Messsystem mit zwei individuellen Messpunkten entworfen, verbaut und auf dessen Kapazitäten getestet. Mit diesem System wird in weiterer Folge der triboelektrische Effekt bei verschiedenen Drücken charakterisiert, wobei besonderer Fokus auf das theoretische sowie experimentelle Entladungsverhalten gelegt wird. Schlussendlich wird thematisiert, ob thermische Desorption von Ionen prinzipiell möglich ist. Dabei werden experimentell erhobene Daten präsentiert, welche die Machbarkeit jener Desorption nahelegen.

Abstract English

If two electrically neutral materials are brought into contact, an exchange of charge can occur. This effect, called tribocharging, has been known for over 2000 years, yet its mechanism is still poorly understood. Perhaps one of the most puzzling questions is the identity of the charge-carrier itself. While it is often assumed that the carriers are electrons, they could also be ions, and different experiments in different circumstances provide suggestive evidence for both cases. In order to address this fundamental issue, we develop an experiment with the end goal to undoubtedly determine the role of ionic charge transfer in insulator contact charging. Since ions are best differentiated from electrons by their huge mass difference, a mass spectrometer is utilized. The experiment is planned as follows: An insulating sample is charged up *via* contact with another sample before facing the entrance of a mass spectrometer. Afterwards the sample's temperature is increased, which could lead to thermal ionic desorption. If the amount of thermally desorbing ions can be correlated to the total charge exchange, the existence of ionic charge carriers in contact charging would be undisputed.

In order to arrive at this stage of the experiment, a number of unresolved issues have to be addressed first, representing the subject of this thesis. Apart from setting up the experiment in general, the first primary task is given by the need of a suitable contact-less charge measurement system. For this, a system is designed, built and tested for its capabilities. Two separate measurement points are in place in order to ensure the charge exchange is accurately tracked. Said system is then utilized to characterise the behaviour of contact charging at different pressure levels, putting special focus on the theoretical as well as the experimental discharging behaviour. Lastly, the feasibility of thermal ionic desorption in general is discussed, including preliminary experiments that support the idea of said desorption.

Contents

1. Introduction

When two materials come together to form a contact, they exchange some electric charge. This effect is called the triboelectric effect, contact electrification or tribocharging and arises independently of the materials used (1). While the case of conductor-conductor interactions is sufficiently understood using the concept of a work-function (2), the charge exchange mechanism behind insulator-conductor or even insulator-insulator contacts is yet to be found. Even though the triboelectric effect has already been mentioned over 2000 years ago (3), there are still many unanswered questions, perhaps one of the most important ones being the identity of the charge carrier itself. The origin of this question is quite simple: after a contact, one material charges negative, the other material charges positive. For that to happen, charged particles must have had traveled from one surface to the other during the contact. Which types of particles are involved in this process?

To address this question, we begin to set up an experiment with the long term goal to show whether ions are involved in contact charge transfer. The idea goes as follows: To cause charge transfer, two samples are brought into contact, afterwards the charge exchange is measured. After contact, one sample is placed close to the entrance of a mass spectrometer and heated up. At this point, ions could desorb from the samples surface. If this is the case, they can be measured with a mass spectrometer. If the number of ions measured this way can be correlated with the total amount of charge transferred, the existence of ionic charge transfer is strongly suggested. However, for this technique to be successful, important experimental details have to be investigated more thoroughly first, constituting the subject of this thesis.

To begin with, a contact-less charge measurement system that includes two independent measurement points suitable for these purposes is designed and tested. Charge exchange at different pressure levels is analyzed and put in context regarding the usability of this experiment. Further on, as a mass spectrometer only operates under vacuum conditions, we investigate the behaviour of charged surfaces under varying pressure. By combining Paschen's law (4) with electrostatic principles, we propose a simple theoretical model regarding the interplay of gas pressure and charged surfaces, which is then compared to experimental data. Additionally we discuss whether thermal desorption of ions trapped at a sample's surface is experimentally feasible - constituting the foundation of the mass spectrometer analysis. All of these points are foundational work towards shining light on the role of ions in the triboelectric effect with this experiment in the future.

2. Scientific Background

In this section, a brief theoretical background on selected relevant topics are given. This includes a theoretical approach to contact electrification between different types of materials, the interplay between charged surfaces and pressure as well as a brief introduction to adsorption/desorption theory.

2.1. Contact Electrification

Contact electrification or tribocharging is the emergence of charge exchange when two materials are brought into contact. This type of charge exchange can be observed when performing conductor-conductor, conductor-insulator or even insulator-insulator contacts (3). On top of that, even a contact between identical insulating materials in terms of their chemical characteristics can be observed (5). So far, there is no theoretical model that accurately describes this effect across all materials (3). Nevertheless, the charge exchange between two conductors is sufficiently understood using the concept of a work function. This model will be briefly introduced in the following, followed by an introduction to charge transfer involving insulators.

2.1.1. Charge Transfer Between Conductors

Conductors are materials that have a high electric conductivity in all directions. A basic but useful microscopic model to understand several aspects of conductors is the "Free electron model", partially developed by Arnold Sommerfeld. According to this model, the nuclei of the atoms that make up a conductor have fixed positions across a periodic lattice. While all electrons that belong to a filled shell remain localized around their nucleus, the valence electrons can freely move around and form an electron cloud that spans across the whole conductor. In addition to not being bound to their respective nuclei, the valence electrons can also fully leave the material once they gain more energy than a specific value characteristic to each material. That value is called "Fermi energy" E_F. An electron can gain said energy by a number of different ways, such as photon bombardment (photoelectric effect), increase of temperature (thermionic emission) or external electric fields. The work function W is defined as follows:

$$W = \phi \cdot e - E_F \tag{1}$$

ϕ is the electrical potential outside the conductor and e is the charge of the electron. As W is defined as the difference between the energy acquired by an electron due to an external potential ϕ and the needed energy to escape the material E_F, the electron is able to leave the conductor if $W \geq 0$ and vice versa. In order to predict the direction of charge transfer between a pair of conductors upon contact, their work functions have to be compared. Suppose we have two materials, A and B. If $W_A > W_B$, then B would receive a net charge from A as the energy landscape is shaped such that electrons will transfer more frequently from material A to B than

the other way around (6). While this model is useful in describing the case of two conductors, the work-function concept cannot be adopted to insulators as it relies on electrons being able to freely move around in a material - something they cannot do in an insulator. The next chapter briefly introduces the difficulties that arise with charge transfers between insulators.

2.1.2. Charge Transfer Between Insulators

Tribocharging between insulators can occur between a large variety of different materials. The effect is not only observed between fundamentally different samples, but also with seemingly identical materials regarding their chemical properties (5). Despite there being a lot of proof of the effects existence, a microscopic mechanism to this charge transfer has not yet been found. This also means that the charge carriers involved in the triboelectric effect are still unknown. While some researchers support the idea of electrons being the main contributor to the charge exchange, others favour the concept of dominant ionic charge transfer. While electrons evidently play an important role in the case of conductors (section 2.1.1), their importance in the case of insulating materials is still unclear (3). As electrons are conventionally immobile in insulators due to the existence of a comparatively large band gap, the typical band gap model is insufficient in describing electronic charge exchange. The model can be expanded by so-called "trap states", that sit in between the valence and conduction band, which could explain some aspects of contact charging (7).

Ionic charge transfer is the driving mechanism behind materials with mobile ions, such as ionomers. For insulators without mobile ions, a similar mechanism is often proposed in combination with water layers that cover surfaces, where split up water molecules could bind to the other surface upon contact. Therefore, ions that either originated from the material itself or adsorbed to its surface could prove to be important in the charge exchange between insulators. The importance of the different possible contributions could also vary with changing temperature, humidity, pressure or the preparation of the surface before the contact. In any case, consecutive charge exchange in the same direction with identical materials as observed in figure 2b remains unsolved. A review paper by D. J. Lacks and R. M. Sankaran (1) gives an informative overview on the different charge exchange models currently under discussion.

In an attempt to find order in the charging direction and magnitude between different materials, the "triboelectric series", first introduced by Johan Carl Wilcke in 1775 (8), is commonly used. The list is obtained by measuring how much charge materials exchange through contact with one another. Afterwards, the materials are ordered by charging direction and magnitude of charge exchange. The ordering of the triboelectric series is done one dimensional, meaning that if material A charges negative against material B and B negative against C, A will also charge negative when brought in contact with material C. However, this is not strictly true and examples for loop-like structures have been found (9). There is no exact widely agreed upon version of this ordering, however different versions are usually very similar

(10). One example of a "triboelectric series" is shown in figure 1.

Figure 1: An example of a triboelectric series. Materials towards the right tend to gain positive charge upon contact while materials on the left lose positive charge. The bigger the distance between two materials, the larger the average charge exchange. Material ordering and illustration based on (1).

To illustrate how two samples get charged through contact, figure 2 shows the charge of a Polydimethylsiloxane (PDMS) sample over numerous contacts with a sapphire sample. The PDMS sample starts out with zero charge, and becomes more and more negatively charged throughout each contact. Due to the polarity of PDMS it would be positioned further left on the triboelectric series in figure 1 than sapphire.
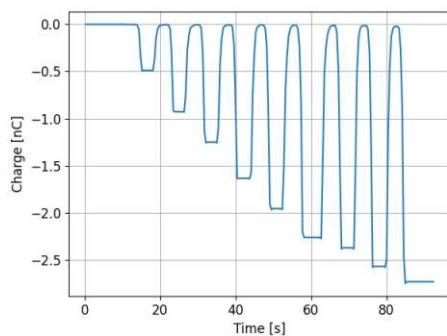
(a) Charge of the PDMS sample, contacts with sapphire.
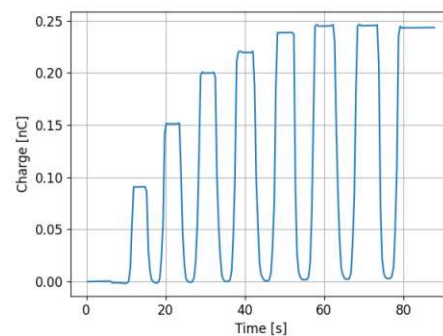
(b) PDMS - PDMS contacts.

Figure 2: Two examples of contact charge experiments. On the left, PDMS is brought into contact with sapphire, on the right with PDMS.

One might imagine the ordering of insulator contact charging with different materials to be the result of some surface property that differs from material to material, leading to more or less charge exchanged depending on the material combination. While that may be the case for different materials, it would imply very little to zero charge exchange for the case of two identical material samples. On top of that, even if there was some charge exchange between identical materials, there would be no clear charging direction since both samples would share the same surface properties.

Nevertheless, experiments done with two identically prepared PDMS samples show that one sample always keeps charging in the same direction. The right plot in figure 2 shows the charge of a PDMS sample upon 7 contacts with another PDMS sample. Evidently, if sample A charges positive upon the first contact, there is a high chance it will turn more positive with each consecutive contact until it reaches a saturation value. Since this behaviour can likely not be explained by the intrinsic material property, it implies the existence of another, yet unknown, external parameter that influences the charging behaviour of materials. This could be *e.g.* something like the roughness of a material or its hydrophilicity/hydrophobicity.

2.2. Pressure Dependence of Charged Surfaces

The following subsection explains why charged objects can experience rapid discharge depending on the pressure level of the surrounding gas.

2.2.1. The Paschen Model

When two separate objects are held at different potentials, a discharging spark can occur once their potential difference V succeeds a specific limit called the breakdown voltage V_B. The value of V_B depends on many factors such as the type of gas between the gap, the gap distance d as well as the gas pressure p. The behaviour of V_B as a function of pressure and distance is described by the Paschen model.

This model is based on the following principles: When an electron collides with a gas molecule at sufficient energy, the molecule has a chance of becoming ionized by releasing one of its electrons (stimulated emission). Due to the presence of an external electric field created by the potential difference of the two materials, the second electron will accelerate along the field lines and has a chance of colliding with another gas molecule, possibly leading to a cascade of electrons traveling along the electric field in one direction and ionized gas molecules following the field lines in the other direction. These free electrons and generated ions are responsible for neutralizing both objects once they reach their respective surfaces. The emergence of this effect heavily depends on the pressure of the gas. If the density of molecules is too high, the mean free path of the electrons (the average distance they travel before colliding with another molecule) is too small to acquire the energy they need to ionize the ions, hence a larger voltage has to be used to speed up the acceleration process. On the other hand, if the pressure is too low, an insufficient amount of molecules is present and the chance of collision is reduced as well, also resulting in a higher necessary electric field to cause discharge. Given that these two effects are competing, a minimum must be formed between the high and low pressure regime. The Paschen model can be used to predict the breakdown voltage purely as a function of pressure if the distance is kept constant (4). Guided by the explanation given above, the breakdown voltage of the gas over pressure is given by

$$V_B = \frac{B \cdot p \cdot d}{ln(A \cdot p \cdot d) - ln(ln(1 - \frac{1}{\gamma}))}. \tag{2}$$

Here, A and B are gas-specific constants that need to be determined experimentally and γ is the second electron emission coefficient of the gas, which provides information about how many secondary electrons are generated when a gas particle is ionized due to collision with another gas particle. The minimum pressure, p_{min}, can be found by differentiating and rearranging equation 2. At *e.g.* a distance of $d = 100$ mm, p_{min} can be estimated using

$$\frac{dV_B}{dp}|_{p=p_{min}} = 0, \tag{3}$$

$$p_{min} = 1.33 \cdot 10^{-1} \text{ mbar}. \tag{4}$$

In this example, $A = 112.5 \frac{1}{\text{kPa·cm}}$ and $B = 2737.5 \frac{\text{V}}{\text{kPa·cm}}$, which are the values for air (11). Equation 4 now tells us that two opposing probes, separated by d, will discharge to a certain degree if $V \geq V_B(p_{min})$ and $p = p_{min}$. Of course discharge can not only happen at p_{min}. As long as $V > V_B$, the voltage is high enough for the gas to turn conductive and develop a spark - p_{min} just denotes the pressure where the least amount of voltage is needed to do so. Figure 3 shows the typical form of equation 2, the breakdown voltage is plotted over $p \cdot d$.
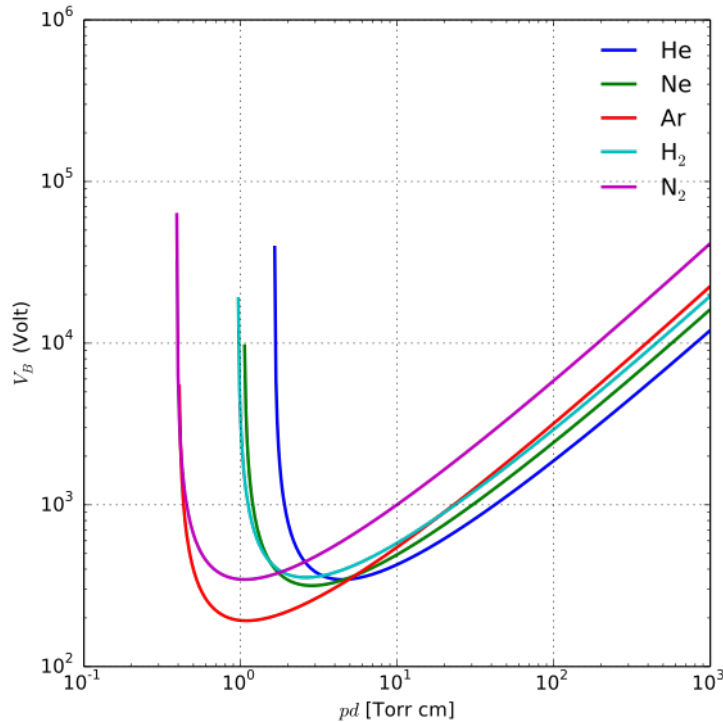

Figure 3: Plot of the breakdown voltage of five different gases as calculated by the Paschen model, taken from (12). License information given in appendix A.

It is noteworthy to mention that discharge can also occur with only one charged object. As long as the electric field is high enough, the gas can become conductive

and discharge the sample the same way as derived above.

2.3. Adsorption & Desorption

Adsorption refers to the attachment of molecules or atoms (sometimes referred to as species) to the surface of a material without penetrating into its bulk, desorption refers to the detachment of previously adsorbed particles from a surface (13). In this framework, the *e.g.* molecules attaching to another material are called adsorbate, the solid underneath is called adsorbent. The reason why species even adsorb to a surface in the first way lays within the way solids are structured. While all atoms inside the bulk material bond with their neighbour atoms, the atoms making up the surface can only form bonds with atoms sitting inside the bulk or their neighbour surface atoms, leaving capacity for outside species to couple. The adsorbate can bound to the surface in different ways, resulting in stronger or weaker bound particles. Hereby, adsorption is usually separated into two groups, the first being called *physisorption*, the second *chemisorption*. A species is physically bound to a surface as long as the adsorbate does not form chemical bonds with the adsorbate. Usually, physisorption refers to the case where an adsorbate is bound to the adsorbant over Van der Waals forces. These forces are typically dominated by dipole-dipole interactions, which are very weak compared to the binding forces that arise in the case of chemical adsorption (14). Figure 4 shows an example of a potential close to the surface, the global/local minima shows chemisorption/physisorption. The dotted lines represent the respective potentials in isolation. The energy barrier a chemically adsorbed particle needs to overcome, in order to desorb, is given by E_{act}.
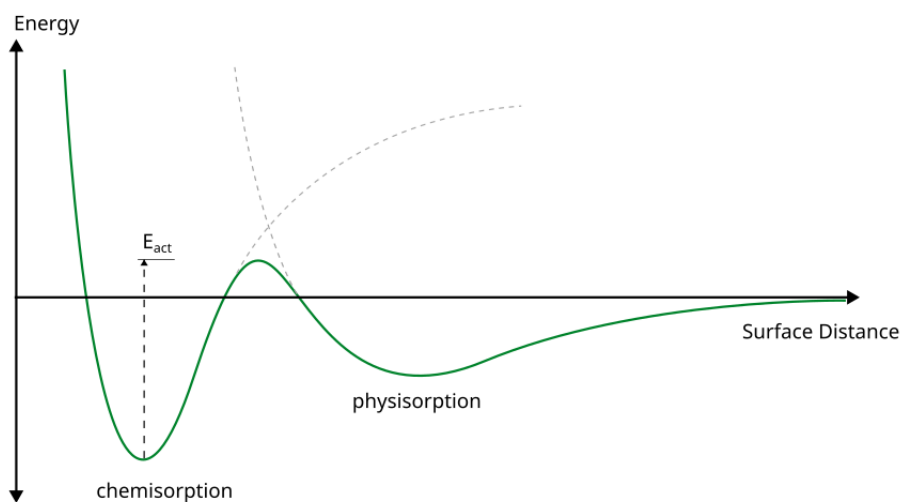

Figure 4: Potential close to a surface as seen by an approaching particle. The energy barrier between chemisorption and physisorption could also be lower than zero. Image based on (15).

The coverage defines how much of a given surface is covered with the adsorbate, where a coverage of 1 corresponds to a full mono-layer. Depending on the available

amount of adsorbate, the coverage can exceed a mono-layer in physisorption. In this case, the previous layer of adsorbate acts as the new adsorbant and forms bonds with the latest layer.

2.3.1. Adsorption Kinetics

Before desorption is discussed, a brief review on how particles adsorb to a surface is given. For this, a model of the dynamic microscopic process at the surface of a material during adsorption is necessary. The ratio between the rate of actually adsorbed particles r_s versus the the flux of particles I impinging the surface of the adsorbant per second is given by the sticking coefficient s,

$$s = \frac{r_s}{I}. \tag{5}$$

A general form of modelling the sticking coefficient s is given by

$$s = \sigma \cdot f(\theta) \cdot e^{-\frac{E_{act}}{k_B T}}, \tag{6}$$

where σ is called the "condensation coefficient", f gives the probability of finding an empty site dependent on the coverage θ and the last term represents the Boltzmann factor. Now the challenge lays within modelling the function $f(\theta)$. The "Langmuir Desorption Model" imposes a few simplifications in order to obtain a useful expression for $f(\theta)$. First off, adsorption of species is limited to one monolayer. Once the coverage reaches $\theta = 1$, no more adsorbants can attach. Furthermore, each adsorption site can only host one adsorbing molecule or atom, afterwards the site is occupied. Lastly, each adsorption site is to be treated equally, there is no energetically more favourable option between two empty sites. Within this framework, the probability of an empty site naturally decreases with an increasing coverage, a plausible form of f is given by

$$f = (1 - \theta)^n, \tag{7}$$

where n dictates the "order of kinetics" which can be pictured as the number of sub-steps it takes a species to fully adsorb to a surface. If, $e.g$, a molecule hits the surface and directly adsorbs to the surface without additional steps, $n = 1$ is used. However, if an impinging molecule were to split up into two parts and occupy two independent sites, $n = 2$ would be more suitable. One can see that the correct choice of n depends on the specific species involved in the process. Non-dissociative adsorption is denoted by $n = 1$, while $n = 2$ refers to dissociative adsorption. The kinetics of a desorption process of one adsorbant can also shift between different orders of n with changing temperature. In dissociative Langmuir adsorption, $f(\theta)$ can depend on the mobility of the dissociative products, introducing the number of empty nearest neighbour sites z as a factor. Products that are mobile can travel along the surface to an empty site that does not necessarily have to be close by, however immobile products require $z > 0$ in order to adsorb (13).

2.3.2. Desorption Kinetics

Desorption can be induced by decreasing the pressure p or increasing the temperature T in a system. By increasing T, the thermal energy of adsorbed particles increases until more and more particles gain sufficient energy to overcome their binding potential and desorb. The desorption rate r_{des} can be modeled in a similar fashion to the sticking coefficient in equation 6,

$$r_{des} = \sigma^* \cdot f^*(\theta) \cdot e^{-\frac{E_{des}}{k_B T}}, \tag{8}$$

where σ^* is called the desorption coefficient and $f^*(\theta)$ is used to describe the coverage dependency of r_{des}. The coverage can once again be expressed in terms of powers n of θ,

$$\sigma^* \cdot f^*(\theta) = k_n \theta^n. \tag{9}$$

As r_{des} is just the rate of change of the coverage θ with respect to time, equation 8 can be rewritten as a differential equation, called the $Polanyi - Wigner\ equation$

$$\frac{d\theta}{dt} = k_n \theta^n \cdot e^{-\frac{E_{des}}{k_B T}}. \tag{10}$$

Here, k_n is the desorption rate constant that also depends on n. Once again, n governs the order of the kinetic process, similar to the adsorption kinetics model discussed in section 2.3.1. A desorption rate that is linearly dependent on the coverage corresponds to $n = 1$. In this case, molecules or atoms bound to the surface simply escape their trapping potential once they gain enough thermal energy. Following the same pattern as before, $n = 2$ represents a 2 step desorption process. The higher n gets, the more sub-steps are involved. Solving equation 8 for θ with $n = 0$ yields an explicit expression for θ

$$\theta(t) = \theta_0 (1 - \frac{t}{k_0 \theta_0}), \tag{11}$$

which is linear in t whereby the slope depends on the temperature T. Going from $n = 0$ to $n = 1$, $\theta(t)$ changes to

$$\theta(t) = \theta_0 e^{-k_1 t}, \tag{12}$$

showing an exponential decay. The factor $k_{0/1}$ is given by the form

$$k_{0/1} = k_{0/1}^0 e^{-\frac{E_{des}}{k_B T}}. \tag{13}$$

where k_n^0 is called the n-th order rate constant.

2.3.3. Temperature Programmed Desorption

Temperature programmed desorption, in short TPD, is a technique where the temperature of a sample is gradually increased, such that the adsorbants eventually acquire enough thermal energy to desorb. Typically, the temperature in the system is increased linearly,

$$T(t) = T_0 + \beta t, \tag{14}$$

with β denoting the heating rate. At low temperatures compared to the binding energies of the adsorbant, only very little desorption takes place. Once the thermal energy gets sufficiently large, the desorption rate increases rapidly until the coverage eventually approaches zero, reducing the desorption rate back to zero. Figure 5 shows an example of three simulated desorption curves for different heating rates.
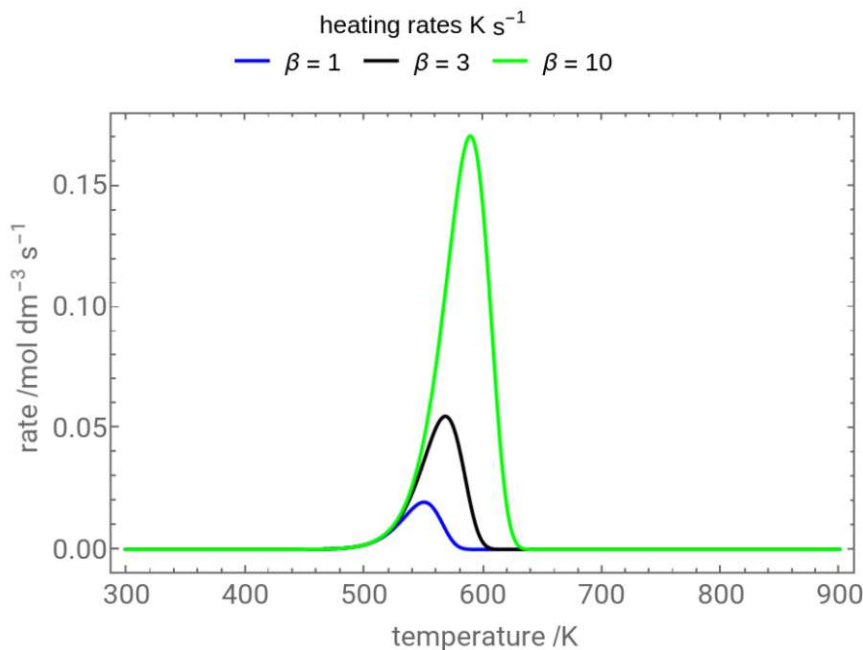
Figure 5: Simulated first order desorption curves using three different values for β, image taken from (16). License information given in appendix A.

Plotting r_{des} over t can be insightful when conducting TPD experiments since they show e.g. the temperature T_m needed to reach a maximum of r_{des}. Contrary to T_m, the desorption energy E_{des} cannot be extracted straight forward out of the plot yet still constitutes an important quantity in the context of desorption. In order to obtain an estimate for E_{des}, the following empirical relationship between T_m and E_{des} is found (17),

$$E_{des} = k_B T_m (\ln(\frac{\nu_1 T_m}{\beta}) - 3.64) , \tag{15}$$

10

where v_1 is the *attempt frequency* with an approximate value of $\nu \simeq 10^{13} \ s^{-1}$. Formula 15 only holds for coverage independent v_1 and E_{des}.

To obtain a more profound estimate of the desorption energy, an *Arrhenius* plot can be used. For this method, r_{des} is measured for experiments where the temperature T is kept constant. For each run, r_{des} and T are denoted. Rearranging equation 8 to

$$ln(\frac{r_{des}}{\sigma^* f^*}) = -\frac{E_{des}}{k_B} \cdot \frac{1}{T}, \tag{16}$$

and using a logarithmic scale for the vertical axis yields a linear graph of $\frac{r_{des}}{\sigma^* f^*}$ as a function of $\frac{1}{T}$. After a sufficient number of experiments, $ln(\frac{r_{des}}{\sigma^* f^*})$ can be plotted against $\frac{1}{T}$ where one experiment corresponds to one data point (18). By fitting the data set to a linear function, E_{des} can be extracted by taking the value of the slope s,

$$s = \frac{-E_{des}}{k_B}, \tag{17}$$

$$E_{des} = -s \cdot k_B. \tag{18}$$

3. Method & Experimental Setup

The first part of this chapter briefly introduces the idea that rest at the core of this experiment and further discusses previous experimental work that explored thermal desorption of ions. Afterwards, a general description of the setup used in this experiment is given, followed by a more detailed description of each relevant part for this project.

3.1. Method and Previous Work

There are various kinds of surface analysis techniques, each with their own strengths and drawbacks. However, as this experiment heavily depends on the detection and classification of ions, the use of a mass spectrometer is essential. Using a secondary ion beam similar to secondary ion mass spectrometry (SIMS) is not an option, as this beam ionizes the surface upon removing it, making it impossible to say whether ions already existed on the surface before the beam. In fact, any technique that relies on excitation through a secondary particle beam introduces said problem in the context of this experiment. For this reason, the possibility of thermal desorption, as explained in 2.3.2, is explored. If thermal desorption is shown to be usable for to detect ions that adsorbed to a surface, the importance of ions within the mechanism of tribocharging could likely be determined as well. For this, a sample will be charged up via contacts with another sample, whereas the exchanged charge is measured. Afterwards, the sample would is heated up while facing the entrance of a mass spectrometer. If one measures an ionic desorption signal, it can be correlated to the amount of exchanged charge that has been measured before. If no ionic desorption signal is measured, it is plausible to assume that ions do not play a significant role in this process and electrons are the dominant charge carriers. This conclusion of course only holds if thermal desorption of ions from a surface is shown to be possible in general, however only little research is conducted on this matter.

A paper published in 1957 titled *Ion Desorption from Metal Surfaces* (19) reports on the thermal desorption of positive nitrogen ions from a tungsten surface. The authors bombarded tungsten with low energy positive nitrogen ions or low energy electrons and observed desorbing ions when heating the surface to 2000 °C after the bombardment. The sample is kept in a nitrogen filled environment at about $7.5 \cdot 10^{-7}$ mbar. No desorbed ions are measured from a surface that has not been bombarded previously. In fact, heating the surface once cleans its surface such that no desorbing ions are measured in consecutive runs until the surface is bombarded again. Since no specifics on the type of desorbing ions are given, it appears their measurement technique was not sensitive to different atomic masses. According to the authors, the measured desorption signals are highly repeatable. The amount of measured ions scales approximately linearly with bombardment time (with electrons or ions) as well as nitrogen pressure. Another paper from 1958 titled *Positive Ion Emission from Metal Surfaces caused by Ion Bombardment* (20) picks up on the results of (19) by using a mass spectrometer to identify the desorbing ions. Their results show that only alkali metals, namely Potassium, Sodium, Rubidium and Caesium, already

present in the sample in the form of impurities, formed the desorbing ionic signal. According to the authors, this occurs due to their relatively low ionization energy, compared to the work function of Tungsten. It is stated that at no times ions that were part of the bombarding beam were detected in the desorption signal, rendering the picture unlikely, that impinging ions loosely bind to the surface to be thermally desorbed later on. Nevertheless, even though leaving open questions as well as dealing with conducting samples instead of insulators, this research demonstrates that thermal desorption of ions from a sample is feasible.

A different paper from 1976 titled *Study of thermal desorption of ions from the surface of β - alumina* (21) presents data on the flash desorption of various elements previously deposited on a β - alumina. Molecules were deposited by sufficiently heating a source close ($\approx$ 3 mm) to the sample and monitoring the ionic current as well as the total amount of charge on the sample. Auger-Meitner spectroscopy showed that the coverage of ions was rather uniform on a 0.3 cm^2 area. The samples were enclosed by platinum foil expect for the ionized surface. The foil was heated up by the use of a high current. By flash desorption they were able to measure very reproducible ionic desorption curves for different elements and ion coverage. The first heat-run after preparing the sample leads to a desorption curve where its shape and size depend on the dosage and the ratio of deposited versus desorbed ions. Figure 6 shows the desorption curves Potassium for a range of dosages, labeled from *a*) to *j*).
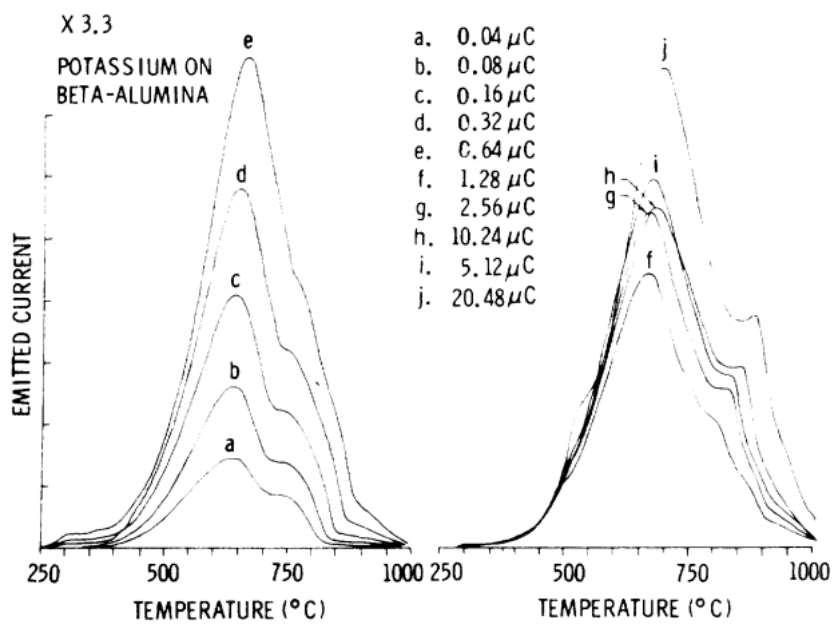

Figure 6: Thermal desorption curves of Potassium deposited on $\beta-$ alumina with different dosages. Reprinted figure with permission from (21). Copyright 2024 by the American Physical Society. License information given in appendix A.

Different runs with different elements and coverage yield different desorption be-

haviour, however, all of the presented data shows that thermal desorption of ions is possible. Nevertheless, since β - alumina is a very complex material, especially in the context of ion transport, further implications on the behaviour of desorbing ions from other, perhaps less complex materials, are not discussed here.

3.2. Setup Overview

The experiment consists of a large cylindrical vacuum chamber with multiple components inside. Two samples are used in order to perform a charge exchange through physical contact, whereas one sample is referred to as the primary or main sample and the other one as the second sample. Both sample positions can be controlled from outside the chamber such that experiments can be conducted without having to open the vacuum chamber. The primary sample rests on a heater that is used to increase the temperature of the sample. The heater is controlled by a feedback loop algorithm to ensure a controlled temperature increase. In order to measure the charge exchanged upon contact of the samples, two separate charge measurement options are installed. The charge of the primary sample can be measured using a Faraday plate. This plate can be slid in front of the sample with very little distance between the sample's surface and the plate in order to measure as much of the sample's charge as possible. The charge of the second sample is measured with a Faraday cup that is placed such that its charge is measured once the sample is fully retracted from the chambers center.

Additionally, the opening of a quadrupole mass spectrometer (QMS) is located inside the vacuum chamber pointing towards the center. The QMS is used to measure potentially desorbing ions when the primary sample is heated up after a charge exchange. Lastly, we use a *photoionizer* to discharge everything inside the chamber before a new experiment is started. The photoionizer is located on a separate second lid that can be placed on top of the chamber in order to discharge all components inside the vacuum chamber. A molecular turbo pump in combination with a roughing pump is used to generate the vacuum necessary to operate the QMS. The experimental setup is shown as a top view in illustration 7.
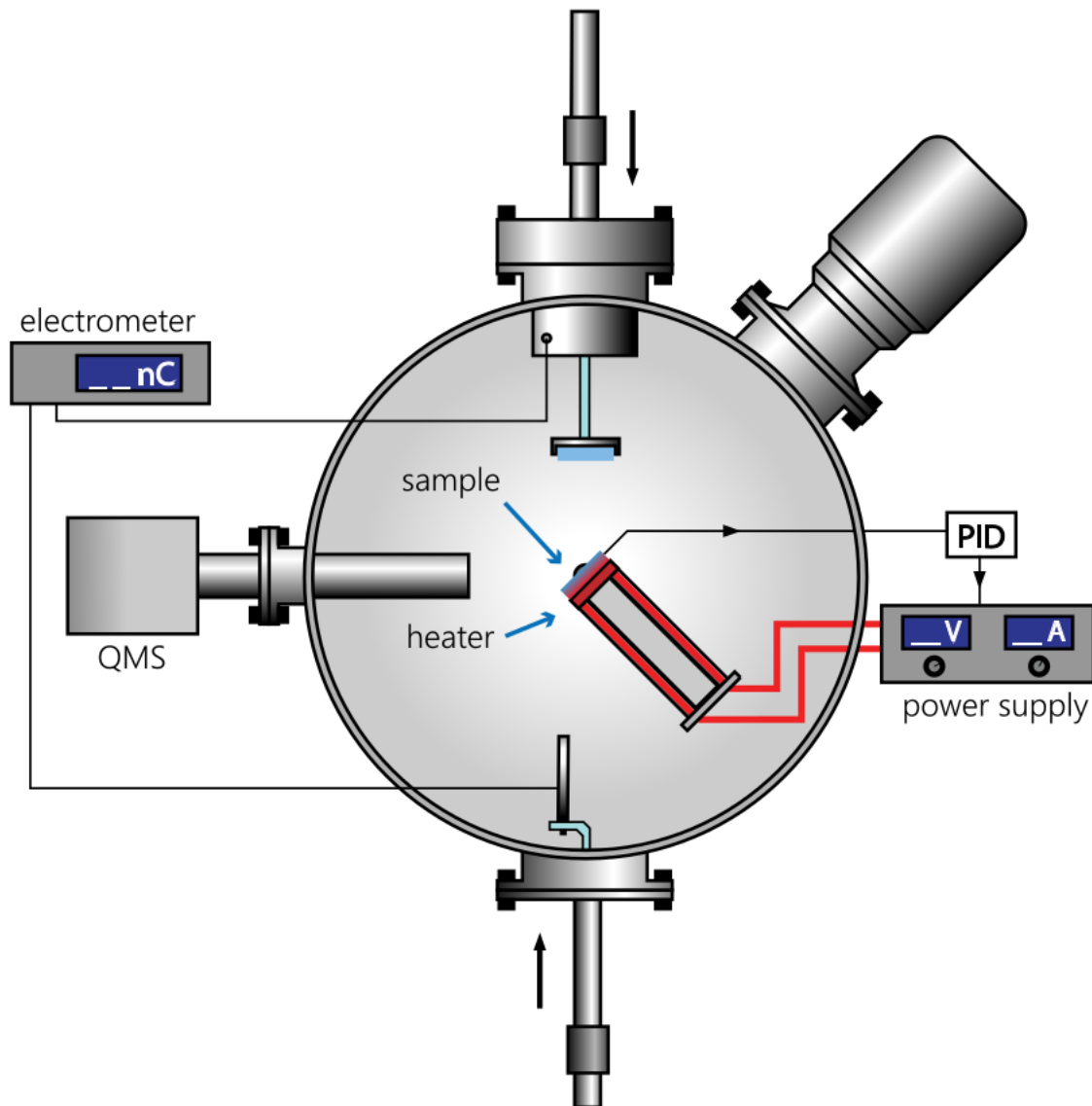
Figure 7: Top view on the experiment. The discharging device is not shown at it is mounted on the inside of the lid.

The following sections go into more detail regarding each part of the experiment.

3.3. Quadrupole Mass Spectrometer

A mass spectrometer is a device that is able to detect charged particles, such as molecules or ions, in their gas phase. The detection works by separating the particles according to their mass-to-charge $\left(\frac{m}{q}\right)$ ratio. There are different kinds of mass spectrometers that use different working principles to achieve this kind of separation. In this experiment, a quadrupole mass analyzer "IDP" by the company "Hiden Analytical" is chosen due to its ability to measure ionic charges with high accuracy (22). The mass spectrometer is used in SIMS mode. This setting is typically used

15

in combination with a secondary ion beam that serves the purpose of removing particles from a surface in order to make the measurable with a QMS. Here, however, no secondary ion beam is used. A QMS consists of multiple different components, the most important ones being briefly introduced in the following.

3.3.1. Ionizer

As the ionizing element is deactivated in this experiment, the following description is kept brief. Mass spectrometers are often used to analyze neutral gases, hence the particles have to acquire some charge before they can be separated by their $\frac{m}{q}$ ratio in the mass analyzer. Therefore, the ion source is used to ionize incoming neutral particles. This can be achieved by a using a cathode and an anode that are placed in a way such that neutral gas particles pass in-between them. By applying a potential difference between the cathode and the anode, electrons are being accelerated perpendicular to the path of the gas particles. Due to collisions between electrons and neutral particles, the latter are ionized and can thus be filtered by the mass analyzer (23).

3.3.2. Mass Analyzer

The mass analyzer is the component responsible for dividing an incoming unsorted beam of ionized particles into separated beams that depend on the $\frac{m}{q}$ ratio of the particles in question. A quadrupole mass analyzer unit consists of four parallel rods that are operated at different potentials. All four rods point along the direction of motion of the incoming ion beam and form a parallelogram like shape in the perpendicular plane, as seen in figure 8.
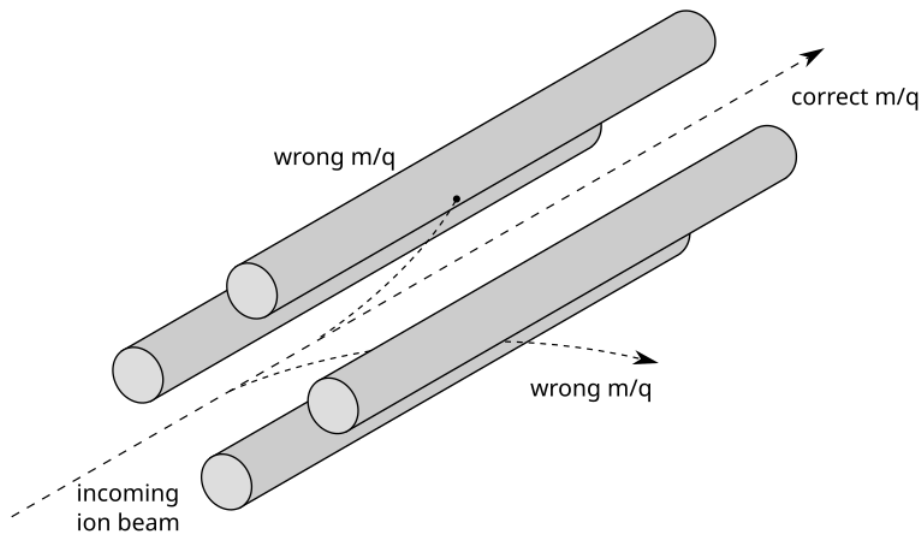
Figure 8: The mass analyzer inside a quadrupole mass spectrometer. Only species with specific $\frac{m}{q}$ values can pass through and reach the detector. Based on (24).

16

Incoming ions travel parallel and along the centre of the rods, where their path is altered from the centered position depending on the present electromagnetic (EM) field. In order to form controllable stable paths, rods on opposite sides are held at the same potential. Between the two pairs of rods, a voltage is applied. This potential difference consists of a DC part U combined with a radio frequency component with amplitude V. This constellation of potentials creates an EM field which affects the pathway of charged particles such that stable paths only arise for specific $\frac{m}{q}$ ratios. The equations of motion that describe the trajectory of a particle in presence of such an EM field are

$$\frac{d^2x}{dt^2} = -2\frac{q}{m} \cdot \frac{U + V \cdot cos(\omega t)}{r_0^2} \cdot x, \tag{19}$$

$$\frac{d^2y}{dt^2} = 2\frac{q}{m} \cdot \frac{U + V \cdot cos(\omega t)}{r_0^2} \cdot y, \tag{20}$$

$$\frac{d^2z}{dt^2} = 0. \tag{21}$$

In these equations, ω describes the frequency of the alternating EM field and r_0 is the radius of the inscribed circle inside the four rods that make up the mass analyzer. The z-axis is aligned parallel to the rods, x and y span the perpendicular plane with respect to z. By using the following substitutions

$$a_x = \frac{8qU}{mr_0^2\omega^2} = -a_y, \tag{22}$$

$$q_x = \frac{-4qV}{mr_0^2\omega^2} = -q_y, \tag{23}$$

the equations 19 and 20 take the same form as the Mathieu equation,

$$\frac{d^2u}{d\xi^2} + (a_u - 2q_u cos(2\xi)) \cdot u = 0. \tag{24}$$

The Mathieu equation has stable and unstable solutions, the latter describing paths where the amplitude in x or y increases too rapid, causing a particle to collapse into one of the rods or escape the trap before reaching its end. On the other hand, a solution is called stable when the described trajectory does not start to form increasing oscillations and reaches the end of the mass analyzer. During operation, the parameters $a_{x,y}$ and $q_{x,y}$ are set such that only the particles of interest form stable solutions and thus pass the mass analyzer. As seen in equation 22 and 23, these parameters are ultimately set by the potentials U and V, hence the amplitudes of the AC and DC field can be used to set which $\frac{m}{q}$ ratio the QMS scans for (25) (26).

3.3.3. Secondary Electron Multiplier

An secondary electron multiplier (SEM) is used to amplify the signal of a charged particle that exits the mass analyzer. For this, the incoming charged particle hits a sheet of metal which is coated in such a way that its work function is lowered. This way, the charged particle will cause multiple electrons to leave the metallic surface and travel towards another metal sheet which is prepared the same way. Between two surfaces exists a potential difference such that the electrons are being accelerated towards the second plate. After this process is repeated multiple times, the current of the initial charged particle can be amplified up to a factor of 10^6 (27).

3.4. Vacuum Chamber

The experiment is conducted inside a vacuum chamber. The chamber is mainly needed because mass spectrometers require very low pressure in order to operate. This has multiple reasons. To begin with, the mean free path has to be larger than the distance between the ion source and the detector, otherwise collisions between particles would alter their trajectory during the mass analyzer. The mean free path of ideal gas particles can be calculated using

$$\lambda = \frac{kT}{\sqrt{2}\pi d^2 p}. \tag{25}$$

A maximum pressure of $5 \cdot 10^{-4}$ mbar translates to a mean free path of at least 60 cm, which is enough to pass the mass analyzer collision free. Additionally, low pressure is important to increase the lifespan of the detector. Since the degradation of a detector depends on the total amount of particles they detect, a lower number of ionized gas ions leads to a longer lasting detector. The manual for the QMS used in this experiment recommends a maximum operating pressure of $5 \cdot 10^{-6}$ mbar regarding the detector lifespan (22). Apart from the necessity due to the usage of a QMS, low pressure is also crucial for some parts of the experiment itself. Without low pressure, desorbed ions from the surface of the sample would collide with air molecules and hence not be measurable by the QMS. The vacuum chamber is also equipped with a valve that allows one to vent the chamber with specific gases, offering more experimental possibilities.

3.5. Samples

As the triboelectric effect occurs between a large span of materials, finding a suitable pair of samples is guided by material characteristics and the magnitude of average charge exchange. A higher amount of exchanged charge simplifies various measurements and is therefore preferred. As the main sample needs to withstand high temperatures, its thermal characteristics are of importance. Charge carriers on conducting samples would immediately rearrange or flow off the sample, therefore insulating materials are necessary. Additionally, the thermal conductivity needs to

be high enough to reach sufficient temperatures at the front of the sample by heating its back side. The main sample is an uncoated Sapphire window disk with a diameter of $d = 25.4$ mm and a thickness of $h = 5$ mm by the company "Thorlabs" (28). Due to its high melting point of 2050 °C, low thermal expansion of $9 \cdot 10^{-6}$ $\frac{1}{K}$ (measured at 1000 °C), good thermal conductivity of 25.12 $\frac{W}{mK}$ (measured at 100 °C) and high electrical bulk resistivity of 10.11 Ωm (measured at 500 °C), Sapphire is suitable for this experiment (29) (30).

The sample cleaning procedure prior to each experiment goes as follows. The sapphire sample is cleaned in a bath of acetone, followed by methanol and finally water for 30 minutes each. Each step is done with the assistance of an ultrasonic cleaner. As every physical contact potentially deposits unwanted charge on the sample, the samples have to be handled with great care before each experiment. Tweezers are used to transfer samples from their storage container onto the sample holder, where the sample is only gripped on its side.

Since there is no heat involved, the second sample can be chosen with a larger focus towards a high charge exchange for easier signal detection. For this reason, Polydimethylsiloxane (PDMS) samples are used. This combination ensures a large charge transfer as evident in section 4. The PDMS samples are prepared using a 10 : 1 ratio of silicone elastomer base to curing agent. After thorough mixing, bubbles are removed with the use of a rough vacuum for 30 minutes. Afterwards, the samples are cured at 90 °C - 100 °C for 24 hours before being cut into 1 cm^2 squares.

3.6. Sample Holders

As mentioned in section 3.2, two samples are placed inside the vacuum chamber. The primary sample sits right in the center on a rotatable stage, such that it either faces the entrance of the QMS or the second sample. The second sample is placed on a stage that can be moved along the radius of the chamber as indicated in figure 7. Both motions, the rotation of the main and the linear movement of the second sample, can be performed from outside the vacuum chamber due to the use of suited flanges.

3.6.1. Main Sample Holder

The main sample holder is held in place by the heater structure which sits on the rotatable stage in the center, hence the whole unit can be rotated all at once. For the experiments shown in section 4.4, the sample is held in place by a holder out of Aluminum oxide. This sample holder is essentially a disk with a circular cut out in its centre. This cutout is just large enough for a round sample with a diameter of $d = 25.4$ mm to fit inside, the sample's temperature is probed by a sensor that is slightly pressed against the side of the sample. One problem with this design is, however, that the sample is not gripped tightly enough. Therefore it would sometimes tip out upon contact with the other sample. Additionally, placing the

sample inside the holder is challenging as well. For this reason, a new sample holder is developed.

Designing a new holder is not trivial since the experimental circumstances introduce a number of constraints and challenges. Firstly, one needs to be able to load and unload the sample without having to touch its surface. Additionally, the backside of the sample needs to be in close contact with the heater in order to ensure sufficient thermal conductivity. To reduce heat loss, the number of contact points on the side of the sample should be kept low. Nevertheless, the sample has to be gripped tightly since the second sample tends to slightly stick and consequently pull on the main sample when retracted after a contact. The material of the sample holder needs to be chosen in such a way that it does not interfere with the QMS signal when heated up along with the sample. It also needs to be able to withstand high temperatures without melting or drastic thermal deformation. Lastly, the sample holder needs to account for the measurement pin that contacts the sample on the side which is used for the temperature feedback loop.

The holder itself is essentially a ring that is cut open on two spots and reconnected with a spring on one point and a hinge on the other. Parallel to the spring there is an additional setscrew. While the spring exhibits a force that works towards closing the gap, the setscrew can be used to force an opening between the two sample holder parts, increasing the area inside the sample holder. This way, one can load a sample by slightly opening the sample holder and placing the sample inside with tweezers. Loosening the setscrew closes the gap due to the force of the spring. The sample is kept in place by three small contact points - alumina screws that point inwards 120° apart - such that heat loss is kept to a minimum. An insulating material is chosen for the set screws in order to avoid charge potentially leaking off amongst them. A picture of the sample holder is shown in figure 9.

Figure 9: One version of the main sample holder, fabricated out of aluminum for easier prototyping. Cutouts for the tweezers are visible. The white pin on the top is the measurement sensor, on the left side the setscrew and the spring are visible.

In order to load and unload a sample without touching its surface, the sample holder has two cutouts such that one can grab the sample on its side with tweezers. For prototyping, the sample holder material was chosen to be stainless steel or aluminum due to availability and comparatively simple machining. However, electrons that radiate from the sample holder due to thermionic emission could potentially lead to ionization processes that in hand further complicate the QMS measurement. For this reason, in the future, the sample holder will likely be fabricated out of a ceramic like material, *e.g.* aluminum oxide. For experiments that are carried out without using the heater system, the heater can be replaced by a more simplistic sample holder since high temperature resistivity is not an issue. For this purpose, a 3D printed sample holder out of polylactic acid (PLA) is used. Since this holder does not introduce any conductive material into the experiment, it is well suited for sensible charge measurements, as further explained in section 4.3.

3.6.2. Second Sample Holder

The secondary sample sits on a sample holder that can be moved back and forth in a linear fashion. One end position is in the center of the chamber while the other one is exactly halfway inside a Faraday cup on the side of the chamber. This way, contacts with the primary sample can be done in the center, while the charge of the second sample can be measured once it is fully retracted into the Faraday cup. The requirements of the secondary sample holder are less challenging since no heat is involved and no temperature measurements are done. The PDMS holder consists of an insulating teflon rod with a magnet on its end. The tray carrying the PDMS

also has a magnet and therefore connects to the rod.

3.7. Temperature Control System

As the temperature of the sample needs to be increased in a controlled manner, a "Proportional - Integral - Derivative" (PID) feedback loop is used. A PID loop is an algorithm that can be used if the value of an output variable $u(t)$ is dependent on a measured variable $T_M(t)$ which should follow a given curve $T_C(t)$. In this case, the output is the power supplied to the heater, the measured variable the temperature and the given curve $T_C(t)$ the desired temperature ramp to a specific set point. The algorithm calculates $u(t_{i+1})$ with the information given by the input variable at time t_i, such that $T_M(t)$ follows $T_C(t)$. Here, P stands for the difference between the measured value and the desired value, which is often called the error value $e(t) = T_M(t) - T_C(t)$. The integral of $e(t)$ is called I, whereas D stands for the derivative of $e(t)$. The PID algorithm assigns the P,I and D values a prefactor, K_P, K_I and K_D respectively, and adds them together to obtain $u(t_{i+1})$,

$$u(t_{i+1}) = K_P \cdot e(t_i) + K_I \cdot \int e(t_i) + K_D \cdot \frac{d}{dt}e(t_i). \tag{26}$$

The integration time in the second term as well as all prefactors have to be set individually or can be determined by an automated setup protocol (31). The sapphire sample is heated using a resistive heater that is placed behind the sample. In order to ensure as little heat loss as possible, the front face of the heater is only in contact with the sample without touching the sample holder around the sample. The heater is powered by a power supply that is controlled by the "Eurotherm Model 2408 PID Controller", a device that performs the PID algorithm mentioned above. The temperature is measured by a thermocouple that touches the sample on its side and transfers the signal to the Eurotherm device.

3.8. Charge Measurement

Precise charge measurements of samples are a fundamental part of this experiment. As the triboelectric effect causes materials to exchange charge upon touch, a contactless charge measurement method has to be implemented. Faraday structures have proven to work very good within these restrictions. In the following, a short introduction on Faraday structures is given, followed by the specific setup used in this experiment.

3.8.1. Faraday Structures

A Faraday structure, most commonly in the form of a Faraday cup, is a conducting structure with a large surface area that partially encloses the object to be measured. In order to use a Faraday cup as a charge measurement device, it has to be connected to an electrometer that is suited for charge measurement purposes. The electrometer

in this experiment uses a capacitor with a well known capacitance C, which is placed inside an integrating amplifier feedback loop. As soon as current flows across the connection between cup and electrometer, the capacitor is being charged up and thus develops a voltage V_{out}. The output voltage of the amplifier is proportional to the input voltage which itself is proportional to the input current I_{in}, hence the number of charges flowing per time. Afterwards V_{out} is measured, scaled by the capacitance and shown as the charge Q

$$V_{out} = \frac{1}{C} \int I_{in} dt = \frac{Q}{C}, \tag{27}$$

$$Q = V_{out} \cdot C. \tag{28}$$

As the capacitance C is known to a good degree, the electrometer is able to detect charges down to a range of 1 fC (32), (33). The working principle of a Faraday cup is explained in the following in more detail.

If a charged object is lowered into the Faraday cup, charges on the conducting cup rearrange according to the electric field of the object, until all electric field lines only have a normal component with respect to the surface of the cup. The charge distribution across the surface of the cup can be modeled using the concept of image charges. Image charges that carry the opposite sign charge with respect to the charged object rearrange themselves, until the potential across the inner surface is constant. These moving charges resemble a current that is measured by the electrometer and converted to a charge according to equation 27. Hereby, the amount of charge measured depends on how complete the object in question is enclosed by the Faraday cup. This can be visualized using the electric field of the charged object. Only the field lines that connect the sample with the Faraday cup contribute to the measured charge, all field lines leaving the cup do not. Hence it is impossible to measure the full charge of an object if the Faraday cup has an opening, since a fraction of field lines will always point outwards. This type of charge measurement can also be achieved using a different geometrical shape - as long as the surface is conductive it will attract a certain fraction of the field lines and form image charges. The challenge with complicated structures, however, lays in estimating that fraction and further extracting the real charge of the object based on the total charge captured by the measurement setup.

Apart from a Faraday cup, a Faraday plate is also used in the context of this experiment. A Faraday plate is a sufficiently large flat plate that is placed closely to a charged flat surface. As the plate is conductive, an electric field will develop between plate and sample and the system can be modeled as a plate capacitor. Figure 10 shows a schematic version of the amplifier feedback loop inside the electrometer as well as a Faraday plate close to a sample. Measurement details on the Faraday plate are discussed in the following.
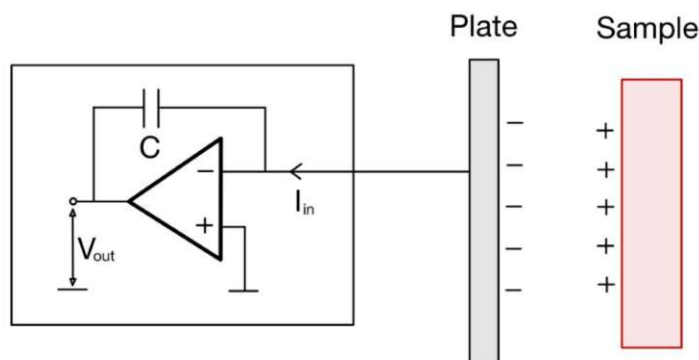
Figure 10: Simplified illustration of an integrating amplifier inside the electrometer to demonstrate working principle of charge measurements with a Faraday plate. Real circuit is of higher complexity.

3.8.2. Charge Measurement Setup

As explained in section 3.8.1, Faraday structures are used to measure the charge of objects. For each sample, a separate measurement option is in place. The charge of the second sample is measured with a Faraday cup that is centered around the outer end position of the sample. Hence once the sample is fully retracted, its charge can be measured. The cylinder obviously needs an opening for the sample to move in and out. In order to enclose the sample as much as possible, the opening is just large enough to fit the sample.

The primary sample is placed on a heater module that consists of many different parts, hence the charge measured by a Faraday cup would not resemble the charge purely of the sample but rather that of the whole structure. For this reason, the signal would be less clear to interpret. Ignoring this difficulty for a moment, it might appear tempting to place a Faraday cup around the sample in order to dynamically measure charge loss as the samples temperature increases. Even though a comparatively large current is used to power the heater, the amount of incoming and outgoing charges should be identical, hence no net charge should be measured by the Faraday cup in response. Nevertheless, a metallic structure surrounding the sample during TPD interferes with the goal to detect potentially desorbing ions with a QMS, since most desorbing ions would fly into the Faraday cup as opposed to exiting the cup. To see this, we look at a single charged desorbing particle that leaves the surface with some initial velocity and is then governed by the electric field built up by the remaining charges on the sample. Of course, this "external" electric field (in the frame of the one desorbing particle) is not constant in time. Since other charges desorb from the surface as well, the field will constantly decrease - nevertheless, as a first approximation, the electric field stemming from the charged sample as a whole is taken to be constant. To demonstrate the problem with a Faraday cup surrounding the charged sample, the following scencario is considered. A charged desorbing particle from the sample surface is modeled by a single charged particle

24

in free space with initial velocity v_0 travelling through a plate capacitor with an electric field E, as seen in figure 11.
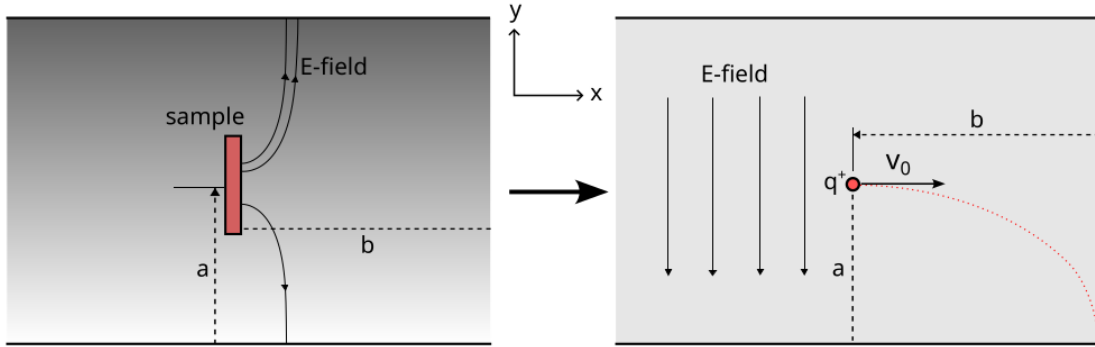
Figure 11: The Faraday cup (left) is approximated by a plate capacitor (right) in order to estimate how much the electric field distorts the path of desorbing ions.

If the sample is sufficiently charged, its electric field will be strong enough such that it can be approximated to be almost perpendicular to the cylinder everywhere expect right in the centre, as demonstrated with the calculations below. For this reason, the approximation by a plate capacitor is reasonable as long as the sample's charge Q is high enough. Now the equations of motion for a charged particle inside a capacitor are solved for the minimum electric field strength E necessary to make the charge collide with one of the plates. The corresponding charge on the sample is given by Q_{min}. The distances a and b are defined in figure 11.

$$a_x = 0 \tag{29}$$

$$a_y = \frac{E \cdot e}{m} \tag{30}$$

$$s_x(t) = v_0 \cdot t \tag{31}$$

$$s_y(t) = \frac{E \cdot e}{m} \cdot \frac{t^2}{2} \tag{32}$$

In these equations, $a_{x/y}$ are the accelerations pointing along the x/y-axis and $t_b = \frac{b}{v_0}$ is the time it takes the particle to travel the distance b in the x-direction. If $s_y(t_b) \geq a$, the particle collides with one of the two plates. One example of this path is sketched in figure 11 on the right side as the dotted red line. Rearranging this equation for E yields

$$E_{min} = \frac{m}{e} \cdot \left(\frac{v_0}{b}\right)^2 \cdot 2a. \tag{33}$$

The initial velocity v_0 is approximated by the thermal velocity $v(T)$ of a free particle,

$$v(T) = 1,6 \cdot \sqrt{\frac{k_B T}{m}}. \tag{34}$$

For 900 °C, this gives

$$E_{min} = \frac{2a}{b^2} \cdot \frac{1.6^2 \cdot kT}{e} = 4.76 \, \frac{\text{V}}{\text{m}}. \tag{35}$$

This translates to a charge of

$$Q_{min} = C \cdot U = \epsilon_0 \frac{A}{d} \cdot d \cdot E_{min} \simeq 4.2 \cdot 10^{-13} \, \text{C}, \tag{36}$$

with $A = 10^{-2}$ m^2. Equation 36 states, that a charge on the order of magnitude of 10^{-13} C on a plate capacitor, as seen in figure 11, is sufficient to stop a particle from leaving the capacitor. Given that the charge exchange upon contact is roughly on the order of magnitude of 0.1 nC = 10^{-10} C (figure 2), it is assumed that charges in the real setup will mostly collide with the cup directly after desorption, rendering a detection with the QMS impossible. As mentioned before, these estimations assume a constant electric field arising from a constant charge of Q_0, whereas in reality the sample's total charge decreases with time, and a more profound estimate on the magnitude of this effect would involve modeling the sample's charge with desorption kinetics, as discussed in 2.3.2. Nevertheless, the mere existence of this effect is enough of a reason to not use a Faraday cup in this way, since a high amount of potentially desorbing ions being able to reach the QMS is crucial.

Therefore, a Faraday plate instead of a cup is used to measure the charge of the main sample. The plate is placed parallel very close to the surface of the sample, such that a large fraction of the charge is picked up. The plate is mounted on a movable stage, this way it can be moved in front of the sample for a measurement and be retracted to the side of the chamber when not in use. In opposition to the Faraday cup, the plate can only measure charge at discrete points in time, *e.g.* once before and once after a thermal desorption experiment. Plate and cup are both separately connected to a "Keithley Model 6514" electrometer. The connection is done using BNC cables where the Faraday cup and plate are connected to the wire in the middle of the cable. On the electrometer side, the Faraday cup and plate are connected with the input low, whereas the vacuum chamber is connected to chassis ground, in accordance with the charge measurement guidelines of the electrometer manual (32).

3.8.3. Modeling the Discharging Process

A charge signal that is obtained using a Faraday plate does not necessarily directly show the actual charge of the sample. The interaction between the measurement device itself with the object to be measured can result in a signal that is not straight forward to interpret, and is therefore easily misunderstood. In order to understand the measurements performed in this context, the interaction between a charged sample, a Faraday plate connected to an electrometer, and the gas of the system, is explained. To model this interaction, a few different quantities have to be introduced. In this model, $Q_P(t)$ is the total charge of the plate and consists of

$$Q_p(t) = Q_i(t) + Q_a(t). \tag{37}$$

Here, $Q_i(t)$ is the induced charge on the plate. This value indicates how many image charges have been drawn to the plate due to the presence of the charged sample. Image charges are essentially the result of charge separation inside a conductor due to the fact, that charges are mobile and rearrange in order to cancel the electric fields inside it. Therefore the value of $Q_i(t)$ only reflects a charge accumulation on the Faraday plate due to the external field, the Faraday plate in total is still neutral - the charge residing on the Faraday plate originates only from charge movement inside the conductor. On the other hand, the absorbed charge $Q_a(t)$ indicates how many additional charges the plate has acquired on its surface. In contrary to $Q_i(t)$, once $Q_a(t) \neq 0$, the plate absorbs physical charges and the Faraday plate itself is not neutral anymore. Finally, $Q_s(t)$ is used to state the actual charge of the sample. The equation

$$Q_i(t) = k \cdot Q_s(t) \tag{38}$$

relates the sample's real charge and the induced charge on the Faraday plate. The fraction of the full charge, that is being picked up by the plate, is given by the efficiency factor $k \in \{0; 1\}$. The more field lines the Faraday structure picks up, the closer k is to 1. In this explanation, the sample-plate system is pictured similiar to a plate capacitor that is connected to the electrometer as illustrated in figure 12.
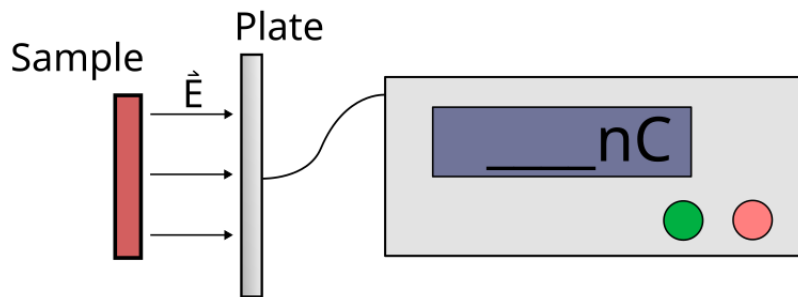
Figure 12: The electric field of the Faraday plate - sample system is modeled as a plate capacitor.

At times $t < 0$, the Faraday plate is assumed to be neutral and there is no charge on the sample. The charge reading on the electrometer does not change when the distance between sample and plate changes as there is no electric field between the two. At $t = t_0$, the sample instantaneously acquires a charge of $Q_s(t_0) = Q_0$. Afterwards, at $t = t_1$, the sample is placed close to the Faraday plate as seen in figure 12, an electric field builds up. The Faraday plate then picks up

$$Q_p(t_1) = Q_i(t_1) + Q_a(t_1), \tag{39}$$

Die approbierte gedruckte Originalversion dieser Diplomarbeit ist an der TU Wien Bibliothek verfügbar
The approved original version of this thesis is available in print at TU Wien Bibliothek.

TU Bibliothek
Your knowledge hub
WIEN

$$Q_p(t_1) = k \cdot Q_s(t_0), \tag{40}$$

where $Q_a(t_1) = 0$. As the sample is now charged, an electric field between the Faraday plate and the sample is present. Now, if the pressure of the system is reduced enough such that the breakdown voltage drops below the voltage built up by the system, $V_B(p(t_p)) \leq V$, discharge can occur as explained in section 2.2. The corresponding time stamp to this voltage breakdown is denoted as t_p, with $t_p > t_1$. Afterwards, at t_2, the pressure is considered to remain below $p(t_p)$ and not change significantly. At t_p, given the object has been sufficiently charged, the gas splits up into ionized molecules/electrons and causes a partial discharge. While charges of the opposite sign of the sample travel towards the sample, the same amount of charges with a flipped sign follow the electric field in the other direction and hit the Farday plate. These charges form the contribution

$$Q_a(t_2) = Q_s(t_0) \cdot d, \tag{41}$$

where $d \in \{0; 1\}$ is the "discharging factor" that states how much charge the sample has lost while undergoing the pressure decrease. If $d = 1$, the sample is fully discharged, whereas at $d = 0$ the electric field was not strong enough to cause any discharge at all. If $d = 1$, the absorbed charges on the plate $Q_a(t_2)$ would be equal to the full charge of the sample before discharge. If now the sample was to be removed from the Faraday plate, the electrometer would still measure this component of the total charge, as it is physically attached to the Faraday plate. The charge of the sample after discharging now becomes

$$Q_s(t_2) = Q_s(t_0) \cdot (1 - d), \tag{42}$$

which would become zero after a full discharge ($d = 1$). The induced charge on the plate takes the form

$$Q_i(t_2) = Q_s(t_2) \cdot k, \tag{43}$$
$$Q_i(t_2) = Q_s(t_0) \cdot (1 - d) \cdot k, \tag{44}$$

which is again just the real charge of the sample scaled by k. According to equation 37, the signal displayed on the electrometer $Q_p(t_2)$ turns out to be

$$Q_p(t_2) = Q_s(t_0) \cdot ((1 - d) \cdot k + d), \tag{45}$$

which is symmetric in k and d and can be rewritten as

$$Q_p(t_2) = Q_p(t_1) + Q_s(t_0) \cdot (1 - k) \cdot d. \tag{46}$$

28

As the factors $(1-k)$ and d are both ≥ 0, $Q_p(t_2) \geq Q_p(t_1)$. This indicates that one can expect the charge reading on the plate to increase after the supposed discharging event between t_0 and t_1 instead of decreasing. At t_2, the sample is now moved very far away from the plate, such that the plate does not pick up any more of its field lines. This causes the induced charge $Q_i(t_2)$ on the plate to vanish and leaves

$$Q_p(t_2) = Q_a(t_1), \tag{47}$$

$$Q_p(t_2) = Q_s(t_0) \cdot d. \tag{48}$$

Using all $Q_s(t)$ equations found so far, it is now possible to plot the samples real charge over the course of an experiment. Both plots in figure 13 do not represent actual data but only show schematic versions of the process. The plot in figure 13a shows what the sample's charge $Q_s(t)$ could look like during pressure reduction.

(a) Charge of the sample

(b) Charge as measured by the plate
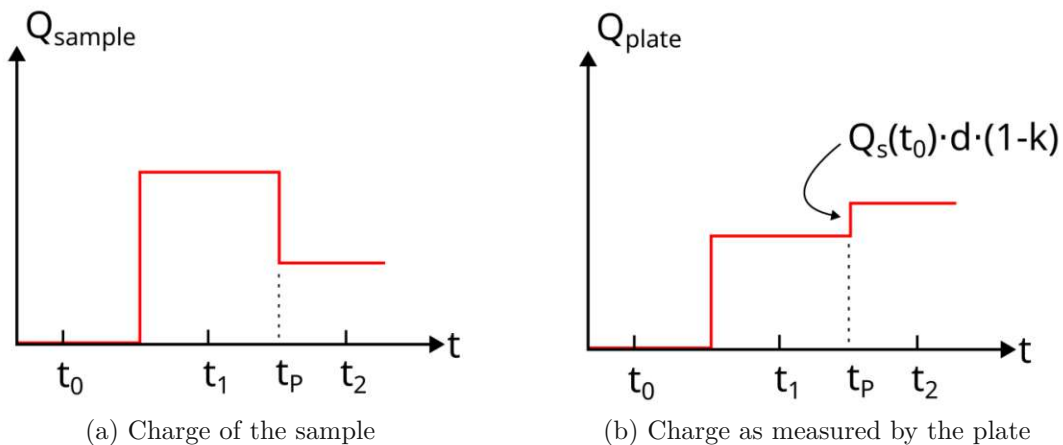
Figure 13: Schematic illustrations of the sample and plate charge following the model discussed here. t_p denotes the time of discharge. Charge loss is quantified by the factor d, k denotes the amount of charge that would be measured by the plate as a fraction of the samples charge.

In 13a, one can see that the charge on the sample does not fully drop back to 0, something that is usually observed in experiments (see section 4.3). This observation is further discussed in section 5.1. The plot in figure 13b shows what the plate would read in such a scenario. As soon as $t = t_p$, the charge (perhaps counter intuitively) increases even further due to the contribution of Q_a.

3.9. Sample Charge Neutralization

The net charge state of two samples prior to a contact charge experiment has an influence on the amount of exchanged charge - a highly charged sample will likely

charge differently from a neutral sample upon contact, as seen in *e.g.* figure 2. On top of that, the repeatability of an experiment calls for an option to discharge samples. Since the mechanism of charge exchange is not yet understood, one has to ensure that the discharging process does not change the surface chemistry of the sample, *i.e.* the surface somehow has to return to its original state after the neutralization. This is important since a different surface structure could potentially exchange charge differently, rendering the experiment unrepeatable. As charged insulating surfaces also experience a natural charge decay, there already is a process that presumably does not alter the chemical surface state more than unavoidable. By simply amplifying an already naturally occurring discharging mechanism, it is assumed that the chemical surface state of the sample is not changed drastically. The mechanism of the discharging process used in this experiment is now briefly presented.

3.9.1. Charge Neutralization Mechanism

Any electrically charged object that is interacting with its environment experiences a charge decay that is governed by three separate mechanisms: (34) conduction of charge through volume, conduction of charge across the surface and the interaction of surface charges with the surrounding gas phase. With the use of an X-ray device, the gas discharge process is sped up such that samples can be discharged on a timescale of seconds. X-rays are produced inside a closed chamber that contains all the objects one wishes to discharge. If the energy of the emitted X-ray-photons is sufficient, a gas molecule can absorb the photon, eject an electron and turn into a positive ion. This electron can further recombine with another stable molecule and form a negative ion. After ionizing the air, ions of the opposite sign with respect to the charge of the sample are drawn towards the sample until the sample is electrically neutral, as illustrated in figure 14. Since positive as well as negative ions are created in the process, the mechanism works with both polarities. The device used to generate said X-rays is characterized in section 3.9.2.
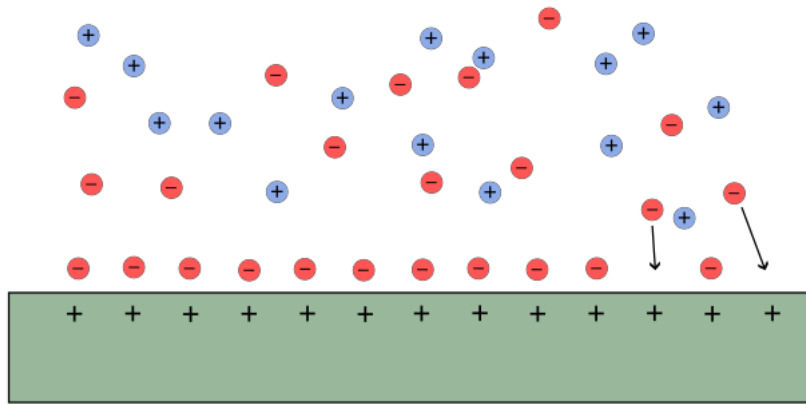
Figure 14: Schematic illustration on the discharging process using gas ions. The charged insulator is shown in green. Gas-phase ions (red/blue) neutralize opposite immobile surface charges of the material. Based on (35).

A simple model to describe the charge decay over time, where a charged sphere only interacts with its surrounding gas phase, leads to an exponential charge decay. By combining Gauss law of electrostatics , the continuity equation and Ohms law (36), one obtains

$$\rho(t) = \rho_0 \cdot e^{-\frac{\sigma}{\epsilon}t}, \tag{49}$$

with ϵ being the permittivity of gas, σ the conductivity of gas ions and ρ_0 the charge of the object at $t = 0$. Equation 49 describes an exponential decay of the charged sphere under the assumption of a constant ion density and a constant mobility over time and space.

3.9.2. X-ray Device

As explained in chapter 3.9.1, samples need to be set to zero net charge prior to each experiment. For this reason, a device called "photoionizer" (Hamamatsu L12645) is used. This device increases the ion density in the surrounding gas, which ultimately leads to the neutralization of charged samples. The device consists of two components, an X-ray head that emits soft electromagnetic (EM) radiation and a control unit that is used to communicate with the X-ray source. When turned on, the X-ray source emits radiation in a cone with an angle of 130°. The energy of the soft X-rays ranges from 3.5 keV to 9 keV. Neutral molecules that are exposed to said radiation can become ionized by interaction with the EM field. Since neutral air is split up into equal parts of positivly and negativley charged species, it is possible to remove positive and negative surface charges from a sample (37). The photoionizer is placed on the inside of the lid of the vacuum hamber. Once the lid is closed, the

whole chamber is filled with ions and discharges rapidly. Figure 15 illustrates the working principle of the photoionizer.
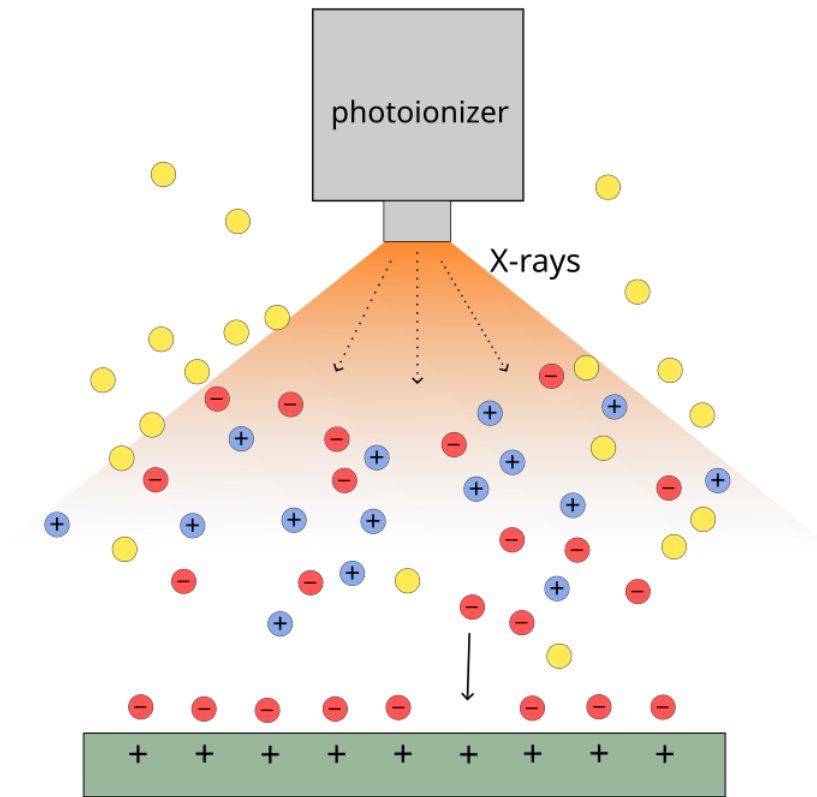
Figure 15: Operating principle of the photoionizer device. The positively charged object is shown in green, yellow spheres represent neutral air molecules and red/blue spheres show ionized air molecules of both polarities. Soft X-rays are emitted within the orange cone. Negative air ions recombine with the positive surface charges until the sample is no longer electrically charged. Based on (38).

The authors of (39) utilized the same device to discharge fused silica grains with a diameter of $D = 0,05$ cm and observe an exponential charge decay with a characteristic decay time of $\tau = 8$ s. Additional experiments done by us show a similar τ for square flat Polytetrafluoroethylene (PTFE) samples of 1 cm^2 in size.

3.10. Camera

Due to the vacuum chamber the experiment cannot be supervised with the naked eye and a camera (IDS model UI-1640LE-C-HQ) is used. The camera is placed outside the chamber attached to a window-seal. It is pointed towards the center of the chamber such that it observes the main sample and thus the contact between the samples (40).

4. Results

In this chapter, the experimental results obtained with this setup are presented. Firstly, the quantification of the charge setup is presented, followed by an analysis on the behaviour of charged surfaces under varying pressure. Afterwards, data obtained with the mass spectrometer is presented.

4.1. Quantifying the Charge Measurement System

Since two different charge measurement options are in place, firstly the capabilities of the system have to be quantified. If the same amount of charge is measured with both methods (Faraday cup and plate, see section 3.8), how much charge does each of them measure? Perhaps more importantly, does the ratio of measured charge remain constant for different amounts of charge?

For these measurements, a PTFE sample is used as the main sample and a PDMS sample as the second one. The PTFE is placed on the purely plastic 3D printed sample holder, since the heater is not needed for these measurements. In the beginning, the whole chamber with both samples already in place is discharged for 13 minutes, long enough to discharge everything inside the chamber to a high degree. Experiments done by us with the same X-ray device in a similar environment show a charge loss of roughly 90 % after 50 s of runtime. By moving the plate over the sample and retracting it, the main sample is confirmed to be uncharged. After exposing the chamber to air for a few seconds, the chamber is closed up again. Now the two samples are brought into contact by moving the second sample towards the PTFE sample. The pressure used to form the contact is observed to have very little influence on the amount of exchanged charge, so long as the surfaces come into full contact. For this reason, the sample holder motion is done manually.

After a contact, the PDMS sample is retracted again, where its charge is now given by the difference between the charge before and after the contact, measured by the Faraday cup. This does not yield 100 % of the sample's charge as discussed in section 3.8.1, however it will be a close approximation since the cylinder is almost fully closed. The charge of the main sample is then measured by sliding the plate in front of the sample and retracting it again after the measurement, giving Q_P. This procedure is then repeated 5 times in order to correlate the two signals. Figure 16 shows Q_P plotted over Q_C, the slope $k = -0.743$ of the fitted linear function (blue) gives the efficiency of the plate in reference to the cup.
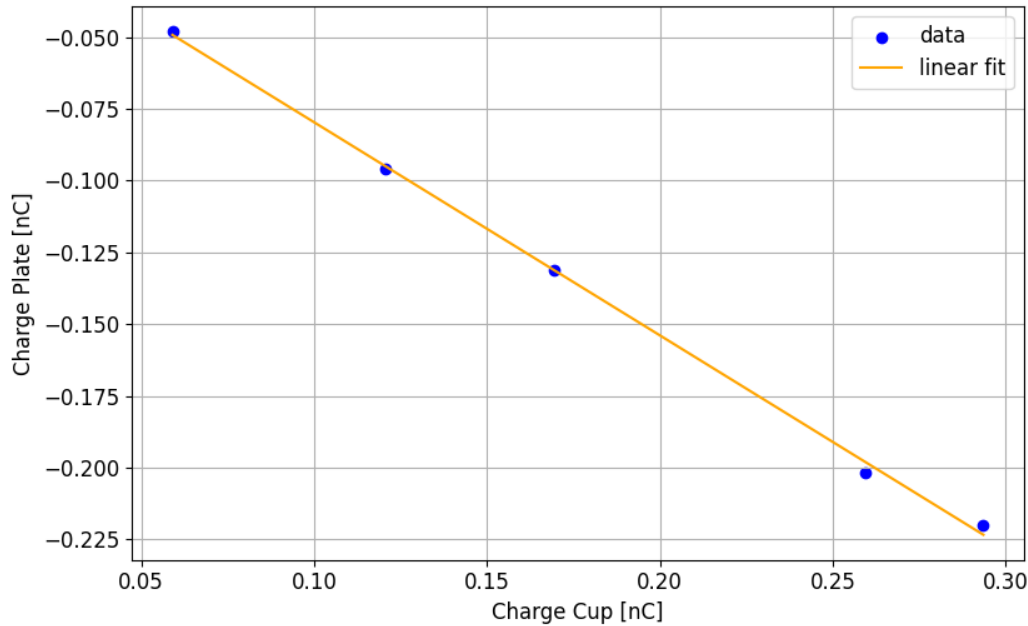
Figure 16: The plate's charge Q_P plotted versus the cup's charge Q_C. Their ratio is given by the slope and turns out to be -0.743.

Figure 16 shows that the plate would measure a charge of $Q_P = -0.743$ nC if the cup were to measure $Q_C = +1$ nC. The linearity of Q_P over Q_C shows that the ratio of charge measured by both systems is independent of the total amount of charge, rendering the system suitable for contact charging measurements. Note that throughout these measurements it is assumed that $Q_A = Q_B$ always holds, where $Q_{A/B}$ is the true charge of sample A/B, hence charge is conserved and no sample dissipates more charge than the other. The slope of 16 can slightly vary if samples or sample holders are swapped, as it heavily depends on the geometry of the system. More importantly, however, is the fact that the ratio remains constant throughout consecutive runs if the setup remains unchanged.

4.2. Charge Exchange Under Vacuum

In order to be able to investigate whether thermal ionic desorption is feasible, a strongly charged sample is required for a higher detection probability. This brings up the question whether the sample contacts should be done in vacuum or at atmospheric pressure before the pump-down. For this reason, both scenarios are measured and compared. The main and the secondary sample are now both PDMS. The main sample is placed on the 3D printed PLA sample holder, whereas the second sample is attached to the secondary sample holder. After the chamber is discharged using the photoionizer, contacts are done between the two PDMS samples. A typical charge curve measured by the Faraday cup can be seen in figure 17.

34
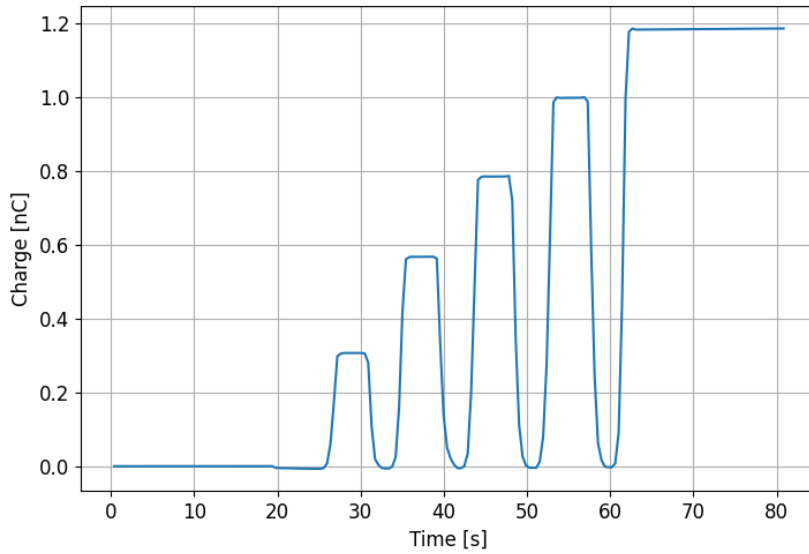
Figure 17: Charge exchange between two PDMS samples. Measured is the charge of the secondary PDMS sample at atmospheric pressure, the samples contact five times.

The measurement starts and ends with the second sample fully centered in the cup, hence the samples exchange a total charge of about 0.89 nC over 5 contacts, which equals to approximately $\Delta Q = 0.18$ nC per contact in atmospheric pressure for PDMS - PDMS contacts. At around 20 s, the second sample leaves the cup and is brought into contact with the primary sample. Since the sample has previously been discharged, the first sample motion can hardly be detected in the charge curve. Once the sample re-enters the cup at around 26 s, the Faraday cup measures its charge. Now the charge reading drops to zero every time the sample leaves the cup and rises to the newly acquired total charge once the sample is returned. Now the charge exchange per contact in vacuum is measured for comparison. Figure 18 shows the charge exchange of PDMS-PDMS at low pressure.
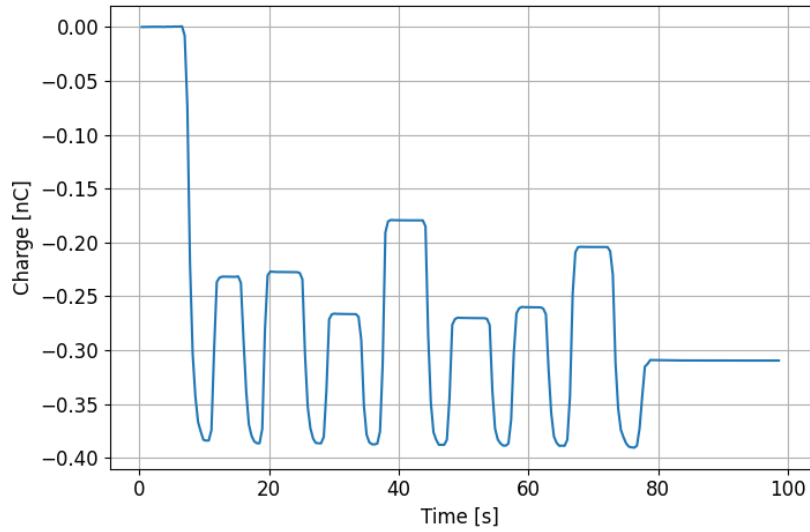
Figure 18: Charge of the secondary PDMS sample in vacuum, six contacts. Some charge exchanges in vacuum show a clear charging direction, others, including this example, do not. The average charge exchange per contact, however, is usually less than at ambient pressure.

The plateaus in figure 18 again correspond to the sample being in the cup, while the dips to -0.39 nC correspond to contacts between the samples. The fact that the dips in both plots, 17 and 18, drop to a constant value, shows that the structure supporting the sample does not get charged over the duration of the experiment. This is a good sign regarding the reliability of this type of measurement. In the vacuum experiment, the charge does not drop to 0 since the sample is still partially charged. Therefore the charge exchange of one contact is given by the difference in height between two consecutive plateaus. During pump-down, the plate is kept in front of the main PDMS sample, therefore it partially discharges as further explained in section 2.2 and 4.3. The contacts are done at a pressure of $p = 1 \cdot 10^{-1}$ mbar, which is below the Paschen minimum of $p_{min} = 5.58 \cdot 10^{-1}$ mbar as calculated in section 4.3. The second sample does not discharge the same way due to a different geometry. The first dip of the blue line around 10 s shows that the second sample still had approximately $+0.39$ nC of charge. The value in figure 18 is negative because the measurement starts with a positive sample inside, hence positive charge is being removed when the sample leaves the cup. The measurement clearly differs from contacts at atmosphere. This manifests itself in a smaller average charge exchange per contact. Apart from the first touch, all contacts lead to a charge exchange $\leq$ 0.1 nC. On top of that, no clear charging direction emerges. The same sample that only charged positive at atmospheric pressure now charges positive and negative in a seemingly random order.

Over different experiments, different charging results in terms of charging direction and magnitude are observed. However, the total amount of exchanged charge in vacuum is observed to be significantly less in vacuum compared to atmospheric

36

pressure most of the time. For clarification it should be noted, that only the primary sample is guaranteed to be discharged during the pump-down process. In contrast to that, the secondary sample's charge is not measured during pump-down and it is potentially still charged. As already mentioned, in the example discussed here, the second sample still holds a charge of approximately 0.39 nC after pump-down. This means that atmospheric contacts are done with neutral samples, whereas the vacuum contacts are performed with some residual charge on the second sample prior to the contacts, giving the impression of an unequal comparison. However, even with slightly charged samples, a much larger charge exchange would be expected at atmospheric pressure than is shown in figure 18. Combining the effect of smaller charge exchange per contact in vacuum with the random charging direction, a smaller final charge on the sample is to be expected compared to atmospheric pressure contacts.

Of course a highly charged sample at atmosphere is not useful for experiments at vacuum if it looses almost all of its charge during the pump-down process as documented in section 4.3. However, it is observed that the sample only discharges to such a high degree if the Faraday plate (or another object) remains fairly close to its surface during pump-down. If the closest thing to the surface of the sample is the mass spectrometer entrance - as it usually would be if thermal desorption were to be performed - the sample does not loose that much charge. This is shown with a sapphire sample placed on the 3D printed PLA sample holder. The sample is charged up by contacts with a secondary PDMS sample. After decreasing pressure below the Paschen minimum, a plate charge measurement shows a decrease of roughly 50%. Experiments show no difference in charge loss between a final pressure of 10^{-5} mbar or 10^{-2} mbar.

4.3. Charge Loss as a Function of Pressure

The breakdown voltage V_B of a gas as a function of pressure is given by the Paschen law, as explained in section 2.2. The graph for V_B yields a minimum for a specific $p \cdot d$ value with a steep increase towards the left of the minimum and a less drastic increase towards higher $p \cdot d$ values. The sample only discharges if the potential difference V between the sample and the plate fulfills the condition $V \geq V_B$. In order to estimate whether this is the case, the sample and the plate are modeled as a plate capacitor. With a separation distance of $d = 3 \cdot 10^{-3}$ m, V can be evaluated using

$$V = \frac{Q}{C}, \tag{50}$$

with C as

$$C = \frac{A \cdot \epsilon_0}{d}, \tag{51}$$

leading to

$$V = \frac{Q \cdot d}{A \cdot \epsilon_0} = \frac{10^{-9} \cdot 5 \cdot 10^{-3}}{5 \cdot 10^{-4} \cdot 8.85 \cdot 10^{-12}} = 1129 \text{ V}. \tag{52}$$

Here, C is the capacitance, $A = 5 \cdot 10^{-4}$ m^2 its area and ϵ_0 the permittivity in vacuum. For the result of equation 52, $Q = 1$ nC has been used. The breakdown voltage V_B is now calculated and compared to the voltage of the plate-sample system. Considering a static geometry, d essentially remains constant and V_B is solely a function of pressure. By calculating the pressure required to reach the minimum of the breakdown voltage using equation 3, one finds

$$p_{min} = \frac{e \cdot ln(1 + \frac{1}{\gamma})}{A \cdot d} = 5.58 \cdot 10^{-1} \text{ mbar}. \tag{53}$$

The numeric values for p_{min} and d can be plugged into equation 2 to obtain V_B

$$V_B(3 \cdot 10^{-3} \cdot 55.8) = 55.84 \text{ V}, \tag{54}$$

which is far less than the 1129 V that the plate-sample system builds up, hence discharge can be expected if $p < p_{min}$. Since here $V >> V_B$, discharge likely occurs at even higher pressures. Solving equation 2 for p and plugging in $V = 1129$ yields a pressure of $p = 8.24 \cdot 10^2$ mbar. This shows that, according to the Paschen equation, a discharge between the plate-sample system is expected to occur at much higher pressures than the minimum pressure calculated by equation 53. (The same logic can of course be applied to smaller Q-values as well. Even a charge of just $Q = 0.1$ nC should generate a sufficient electric field to cause discharge.)

In order to test, whether the theoretical description of a charged sample under vacuum given here as well as in sections 3.9.1 and 2.2 holds, a number of experiments are carried out. In three runs, sapphire is used as the centered sample and PDMS as the second sample. The main sample is placed on a 3D printed sample holder with no conducting materials in place, this way the capacitor system is kept as undisturbed as possible. Prior to each experiment, the system is discharged. Afterwards the samples are brought into contact multiple times whereas the charge of the second sample is tracked with the Faraday cup. The main sample's charge is now measured with the Faraday plate. The vacuum chamber is then pumped down to $p = 1 \cdot 10^{-1}$ mbar, with the plate measuring the sapphires charge throughout the whole process. The plate - sample normal distance with respect to their surface is kept at approximately $d = 3 \cdot 10^{-3}$ m at all times. After the target pressure is achieved, the plate is retracted from the sample, showing the residual charge after pump-down.

This kind of experiment is carried out with slightly different sample holders and different sample combinations, the results are shown below. In order to properly analyze the results, a few more explanations are necessary. In section 3.8.3, k is introduced as the efficiency factor given as the fraction of the full charge that the plate is able to measure. In reality, however, the samples full charge $Q_s(t)$ is not known and the closest approximation available is the Faraday cup charge

measurement. The factor k is now taken individually for each experiment by dividing the first plate measurement in atmosphere with the cup measurement of the second sample, following equation 55,

$$k = \frac{Q_p(t_1)}{Q_s(t_0)}.$$ (55)

As the Faraday cup almost fully encloses the sample, the difference between real charge and measured charge is believed to be small. This means, however, that k is generally slightly overestimated. The discharging factor d, as introduced in section 3.8.3, quantifies the amount of charge loss when the ambient pressure is reduced, and is therefore an important quantity in this experiment. The theory presented in section 3.8.3 allows one to calculate how much charge the sample lost once discharge has occurred. For this, the increase in the charge reading from t_1 to t_2 is used, as seen in *e.g.* figure 19. The size of this increase, now called Δ, can be connected to the total amount of charge lost by the sample (which is quantified by d). In order to achieve this, Δ has to be computed via

$$\Delta = Q_p(t_2) - Q_p(t_1) = Q_s(t_0) \cdot d \cdot (1 - k),$$ (56)

which combines equation 40 and 46. Rearranging this equation results in

$$d_{th} = \frac{\Delta}{Q_s(t_0) \cdot (1 - k)}.$$ (57)

Section 3.8.3 shows that shortly retracting the plate at t_3 relates the initial charge measured with the Faraday cup to the plate measurement using

$$d_{exp} = \frac{Q_p(t_3)}{Q_s(t_0)}.$$ (58)

Therefore d can be measured explicitly (equation 58) as well as calculated from plate measurements at t_1 and t_2 and the full initial charge, $Q_s(t_0)$ (equation 57). Two examples of plate measurements are shown in figure 19, where a number of interesting features stand out.
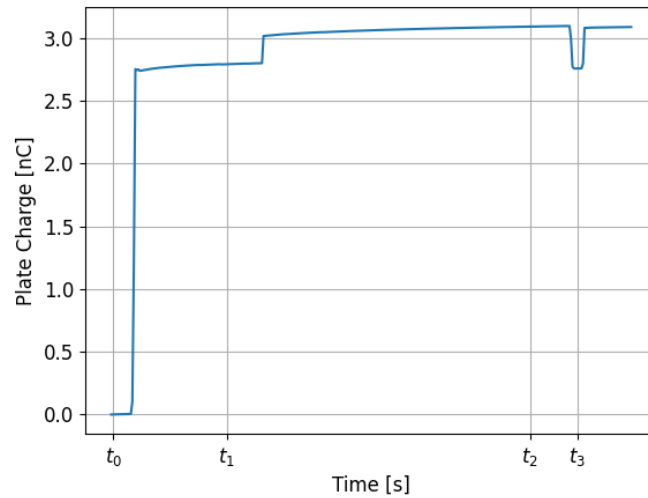
(a) Here, discharge occurs in one step, as seen shortly after t_1.
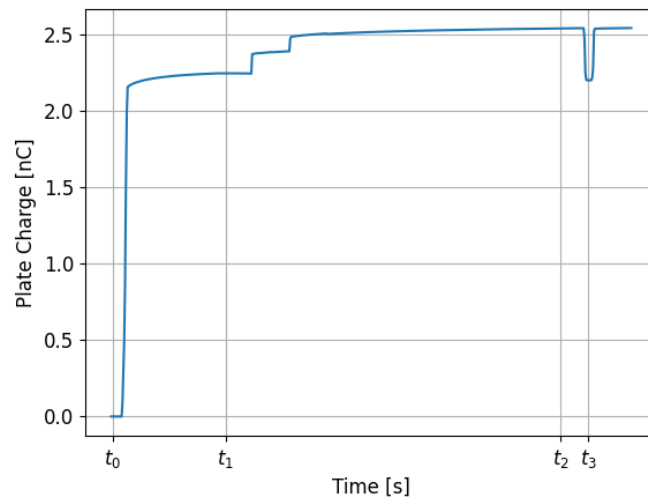
(b) Sometimes the discharge process happens in more than one step.

Figure 19: Two plate measurements of a sapphire sample during pump-down. Data is normalized to 1 for better comparison.

Both curves in figure 19 represent separate, independent experiments. The measurement shown in figure 19a is now shortly characterized. Before $t = 0$, the whole system is discharged. Shortly after t_0, the plate is placed close to the charged sample and measures a charge of ~ 2.7 nC at t_1. Around t_1, the roughing pump is turned on. A few seconds later, the charge reading of the plate increases by a finite value characterized by Δ (equation 56). Sometimes, as visible in figure 19b, this increase is observed to happen in more than one jump. This marks the discharging process of the sample-plate system as the pressure is sufficiently reduced. Even though the plate signal itself does not decrease, the analysis presented in section 3.8.3 shows this increase indeed reflects a decrease in the samples charge. The dip at t_3 arises

40

because the plate is retracted and moved back over the plate in order to measure the residual charge left on the sample. As visible in both plots, the charge slowly changes over time every time a change in charge is measured and appears to drift towards a constant value. After going back to atmosphere, the residual charge is again measured with the plate and shows the same value as in vacuum (not shown in figure 19). In all three experiments carried out with this setup, the plate picks up more than 80% of the full samples charge, with an average k factor of $k_{avg} = 0.84$.

The d values obtained for these experiments are plotted in figure 21 as the first three entities. In all runs, the measured d values are slightly higher than their predicted values.
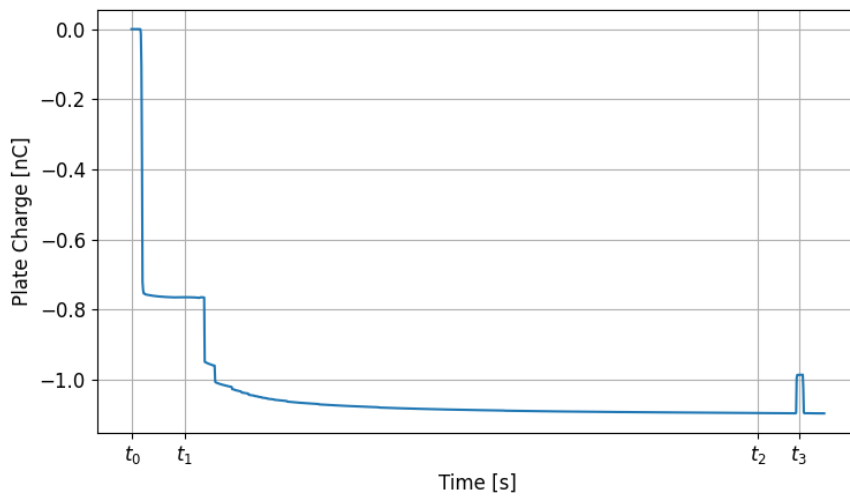
Figure 20: Plate measurement of a PDMS sample during pumpdown.

Now five experiments are conducted with two PDMS samples in place. The main sample is again held by the 3D printed plastic sample holder. These experiments are conducted in the same fashion as with the sapphire sample presented above. Figure 20 shows an example of a plate reading. Again, a similar behaviour as in figure 19 is observed. One obvious difference is the fact that the charge measured by the plate seems to take longer to relax to a certain value once the sample discharges. For reference, in figure 20 $t_3 = 500$ s, whereas in figure 19a, $t_3 = 235$ s. Therefore, the PDMS -PDMS system had close to 500 s to relax into a steady state, more than two times longer than the sapphire system discussed above. Additionally it is observed that the discharge happens in multiple small steps as opposed to a few large steps as seen with the sapphire sample. All k values for PDMS samples are smaller compared to the sapphire values and average to $k_{avg} = 0.629$.

All experimental and theoretical d values for the eight experiments discussed so far are plotted in figure 21.
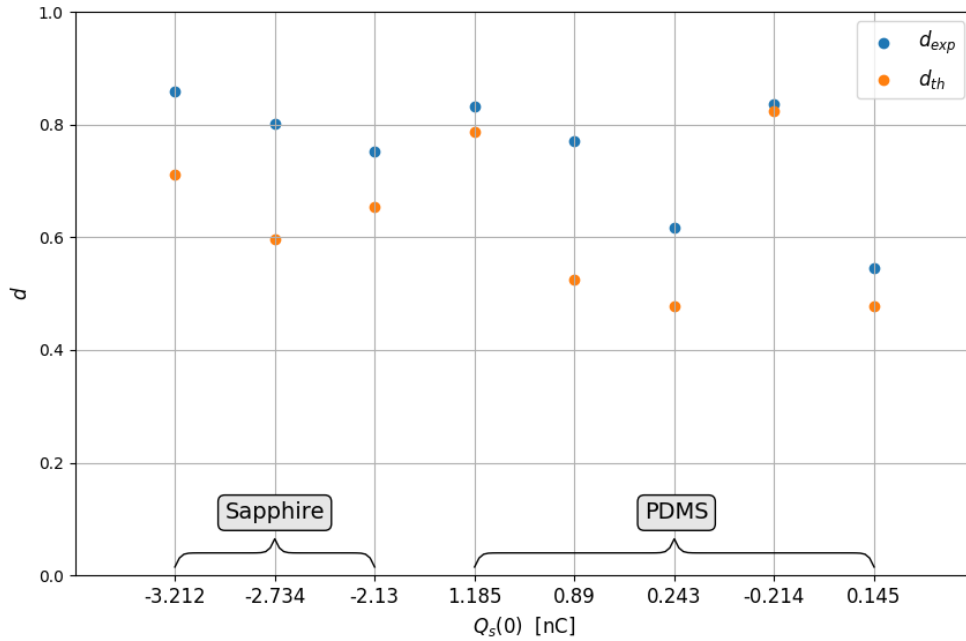
Figure 21: Theoretical and experimental d values for eight experiments. The first three Experiments were conducted with a sapphire sample, the latter ones with a PDMS sample.

In figure 21, the x-axis displays the initial charge of every sample. The experiments are sorted by initial sample charge in descending order, starting with the sapphire sample on the left. One can see that both values for d qualitatively follow the same trend, however, d_{th} is always smaller than d_{exp}. As mentioned in the beginning of this chapter, $Q_s(0)$ is taken from the cup measurement, which will always give a slightly smaller value than the sample's real full charge. However, since $Q_s(0)$ appears in both denominators in the calculations for d_{th} and d_{exp}, this effect cancels out and thus cannot properly explain the observed gap between the measured values. Apart from said discrepancy, d_{th} and d_{exp} clearly behave in a similar fashion. Additionally, the difference between d_{th} and d_{exp} does not seem to depend on the initial total charge of the sample, otherwise that dependency would be observable going from left to right as the initial charge gradually decreases.

Since the model discussed here allows one to calculate the real samples charge at any given point in the experiment, the plate data can be transformed to actual sample charge, which is far more intuitive to interpret. To give an example of this, figure 22 shows the calculated sample charge (blue) from the measured plate charge (orange).
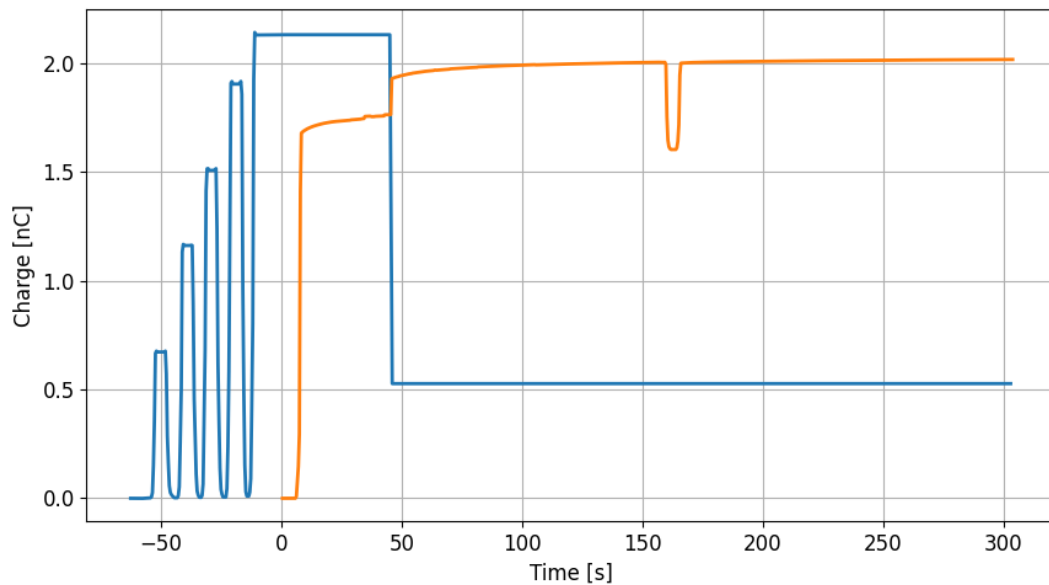
Figure 22: The sample's charge in blue as calculated from the plate measurement in orange.

The blue graph at $t < 0$ shows the charge up progress directly taken from the Faraday cup measurement with a flipped sign to represent the main sample. During the contacts between the samples, the charge of the main sample does of course not drop to zero - this stems from the charged second sample having to leave the Faraday cup every time a contact is done. Afterwards, Q_s remains constant until the pressure is reduced sufficiently. Shortly before $50\ s$, the sample partially discharges and the sample's new charge is given by $Q_s(t_2) = Q_s(0) \cdot (1 - d_{exp})$.

4.4. Ionic Thermal Desorption of Charged Surfaces

In this section, results obtained on the desorption of ions from surfaces, that have been charged up via contact, are presented. As discussed in section 3.1, little experimental research has been published on this matter so far. Nevertheless, some studies on desorbing ions have been conducted, all of which show that thermal desorption of ions in certain scenarios is feasible. In contrast to (19),(20) and (21), the surfaces used in this experiment are not bombarded with an external ion source. Instead, charge is exchanged by contact with another sample. If ions make up a part of the charge carriers responsible for this charge exchange, perhaps it is possible to thermally desorb them afterwards. No definite results on ionic desorption in the context of this experiment can be given, since the task of this project was merely to set up and test the measurement chain leading up to potential results in the future. Definitive results would require more experimental work and a more thorough data analysis. Nevertheless, some preliminary results that appear interesting in the context of thermal ionic desorption are presented.

43

4.4.1. Estimated Signal Magnitude

If a samples charge Q is purely made up of N singly charged ions, the number of ions is given by

$$N = \frac{Q}{1.602 \cdot 10^{-19}}. \tag{59}$$

The total amount of ions measured with the QMS cannot therefore not exceed N of equation 60, if no other ion source is present. For a charge of 1 nC, this would translate to $N = 6.2 \cdot 10^9$ Ions. Additionally, one has to account for the opening angle dictated by the size of the QMS entrance. Dividing the area made up of the opening angle A_{qms} by the area of a half sphere A_{total} (all possible directions ions can take after desorption) gives a rough estimation for the fraction of ions that would travel towards the QMS, given that all directions are equally likely. Mathematically, this fraction is given by

$$\frac{A_{qms}}{A_{total}} = \frac{\int_{\Phi=0}^{2\pi} \int_{\theta=0}^{\theta_0} r^2 \cdot sin(\theta) \, d\theta \, d\phi}{4\pi r^2 \cdot \frac{1}{2}} = 1 - cos(\theta_0). \tag{60}$$

For a sample - QMS distance of approximately $l = 7$ cm and a circular opening of the QMS with a diameter of about 2 mm, the opening angle θ_0 equals 0.014° and equation 60 yields approximately

$$\frac{A_{qms}}{A_{total}} = 10^{-4}. \tag{61}$$

For 1 nC of charge, this would result in an estimated amount of

$$N(l = 7) = 6.2 \cdot 10^9 \cdot 10^{-4} = 6.2 \cdot 10^5 \tag{62}$$

ions to be counted wih the QMS. For some measurements, the sample is set closer to the QMS by 25 mm in order to potentially increase the desorption signal strength. This increases the estimated number of ions that enter the QMS to

$$N(l = 4.5) = 6.2 \cdot 10^9 \cdot 2.5 \cdot 10^{-4} = 1.5 \cdot 10^6. \tag{63}$$

Of course these values only provide an estimation for the relevant order of magnitude in these measurements. A more profound analysis would - amongst other things - include dropping the assumption of angular independent desorption.

4.4.2. Mass Spectrometer Results

To begin with, a sapphire sample is placed on the resistive heater, held in place by a ceramic cylindrical structure. The spring-loaded temperature sensor slightly presses down onto the side of the sample. Since the sample rests in a vertical position, the

force exerted by the spring of the temperature sensor is not sufficient to ensure the sample does not drop out of the holder. For this reason, two small metallic pins cover the edge of the samples surface, prohibiting the sample from falling out. Now the sample is heated to slightly above 500 °C in an attempt to clean its surface. In order to investigate the possibility of water molecules that adhere to the surface being involved in the triboelectric effect, the QMS is set to measure (singly positively charged) atomic masses of 1 (hydrogen), 16 (oxygen), 17 (hydroxide), 18 (water) and 19 (hydronium). Figure 23 shows that only a tiny amount of ions are measured during this experiment within this temperature range. The green line represents a $\frac{m}{q}$ ratio of 1, which would correspond to single protons if only singly ionized species are taken into consideration.
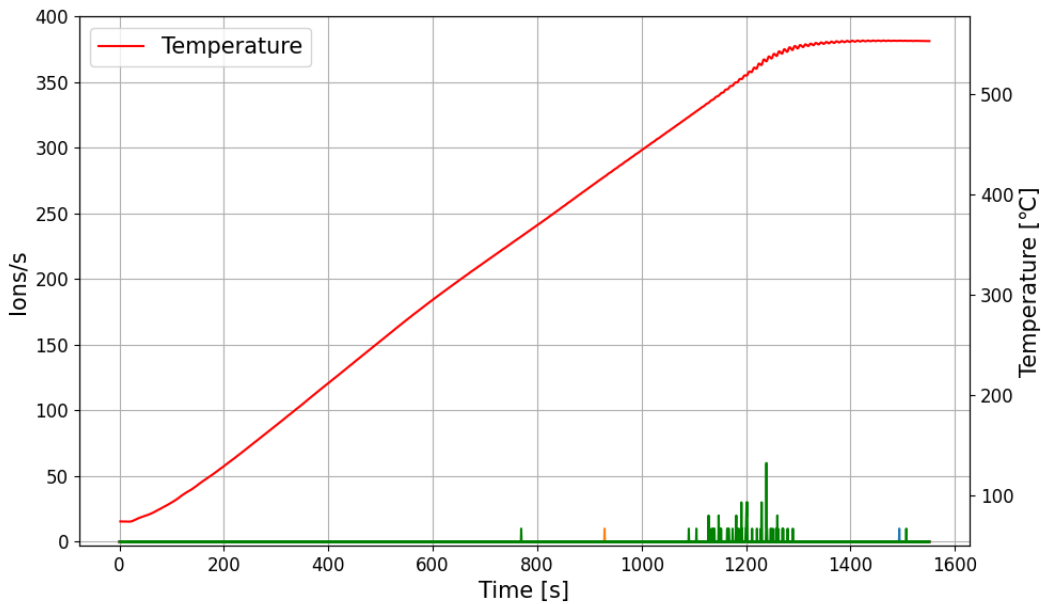
Figure 23: QMS measurement with no sample contacts. The green data represents $\frac{m}{q} = 1$.

Now the sytem remains at low pressure and the temperature relaxes to 70 °C. At this point, contacts with a PDMS sample are performed at a pressure below $5 \cdot 10^{-5}$ mbar. Afterwards, the sample is heated again and the QMS is used to measure the flux of the same atomic masses as above. Figure 24 shows that almost no ions are measured in this case.
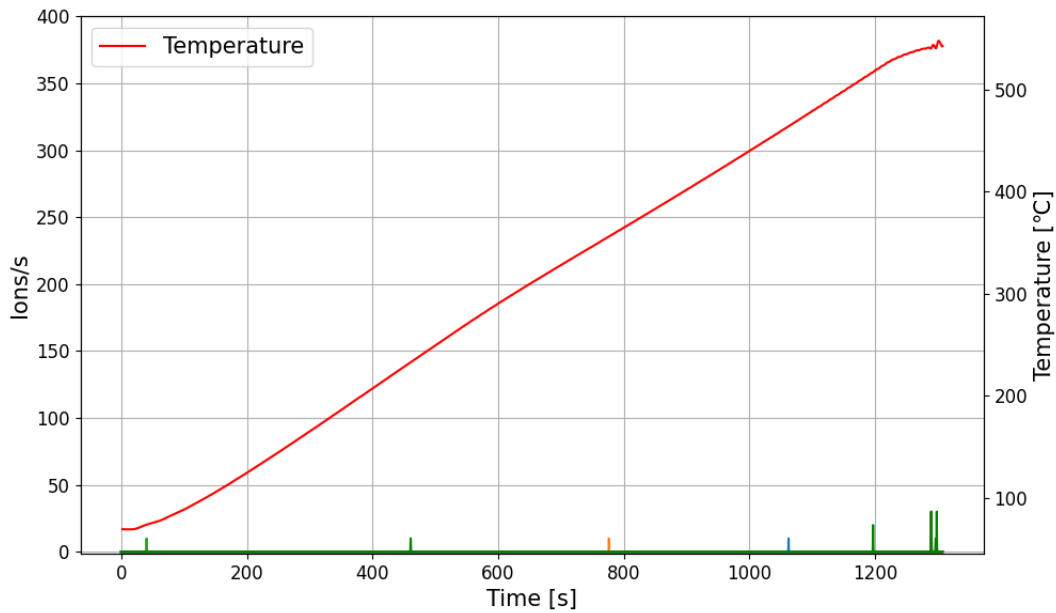
Figure 24: Contacts between sapphire and PDMS are done in vacuum. Almost no ions are measured with the QMS once the sapphire is heated.

Now another set of contacts are performed with the same PDMS sample, this time at atmospheric pressure. Before the sample is heated again, the sample holder is moved closer to the QMS entrance by 25 mm to increase the aperture angle. This way, if ions were desorbed, they should produce a larger signal. Using equation 63 shows the expected signal is amplified by a factor of 2.5.

The sapphire is heated again to almost 400 °C, the results are shown in figure 25. This time, a number of positive hydrogen ions are detected. Even though the signal is of low strength compared to the estimations in 4.4.1, it might resemble a desorption process.
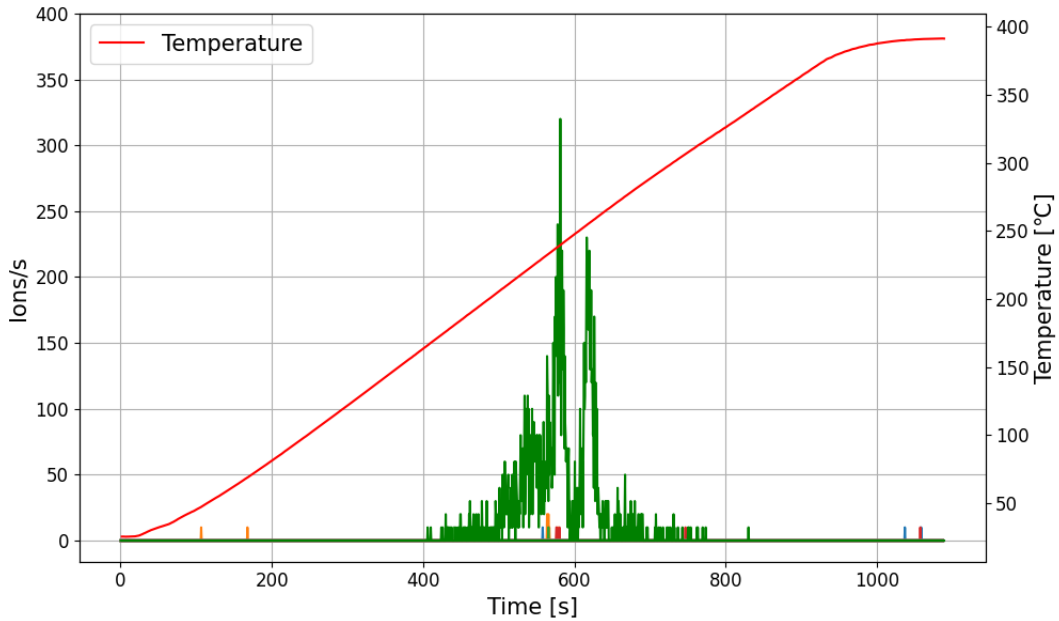
Figure 25: After contacts at atmospheric pressure, a significant amount of ions with $\frac{m}{q} = 1$ are measured.

Even though the sample has been set closer to the QMS only for the atmospheric-contact experiment, this factor does not account for the difference in measured ions compared to the vacuum contacts-/ no contacts- scenario as calculated in section 4.4.1.

To further elaborate on the observation that no significant ionic signal is measured for samples that are contact charged under vacuum, another measurement is presented. Similarly as before, contacts between a sapphire and a PDMS sample are carried out. The PDMS acquires negative charge of approximately -2 nC, hence the sapphire is positively charged. Now the sapphire is heated up again, the QMS measurement is shown in figure 26.

47
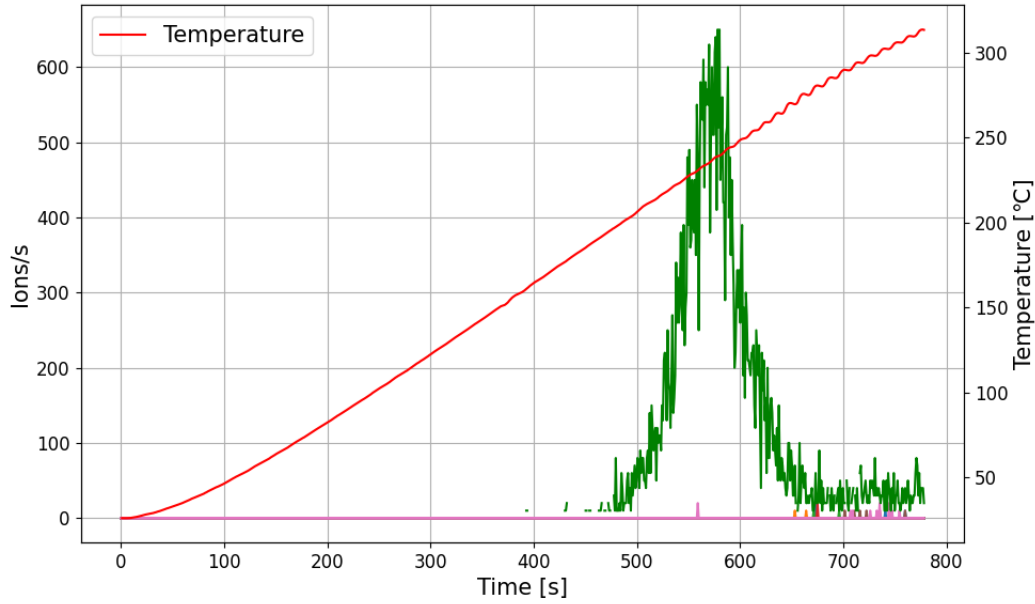
Figure 26: Sapphire-PDMS contacts carried out at atmospheric pressure again lead to a larger amount of measured ions with a $\frac{m}{q}$ ratio of 1.

Again, the QMS measures a significant amount of positively ionized hydrogen. In total, $4.8 \cdot 10^5$ hydrogen ions are measured. By extracting the peak temperature in figure 26, one can estimate E_{des} using equation 15, which results in

$$E_{des} = 1.75 \,\text{eV}. \tag{64}$$

Afterwards, the vacuum chamber is brought back to atmospheric pressure and pumped down again. At a pressure of $5 \cdot 10^{-6}$ mbar, another set of contacts are performed. This time, the sapphire charges negative to approximately -3.5 nC, therefore the QMS is set to measure negative ions. Figure 27 shows the measurement of the subsequent experiment, again almost no ions are measured.
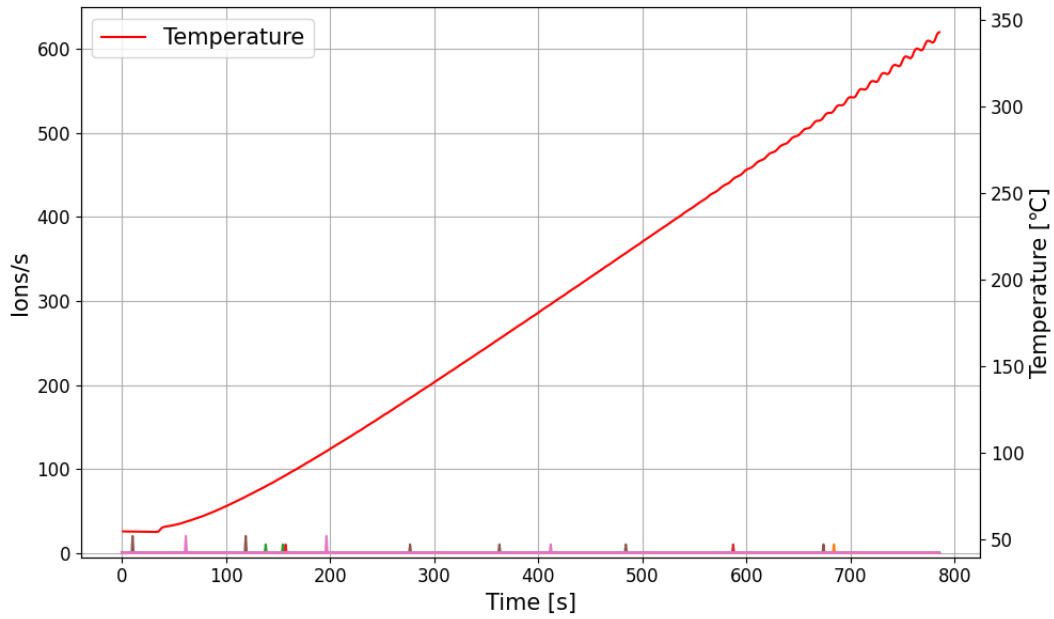
Figure 27: Similiar to figure 24, sample contacts are done in vacuum and lead to no desorption signal.

Higher temperatures have not been reached due to instabilities in the temperature control chain. Even though the signal displayed in figure 26 appears promising, it is important to note that we did not manage to reliably reproduce this measurement - some experiments showed hints of desorption processes while others did not. On top of that, it is not yet attempted to interpret these results in a microscopic manner as this would require more data to work with.

5. Discussion & Outlook

In this section the results presented in section 4 are further discussed and interpreted. Potential problems and challenges that might require a more differentiated approach are presented. Furthermore, promising changes in the setup that could resolve some issues as well as possible experiment ideas are proposed.

5.1. Charge & QMS Measurements

Starting out with the charge measurement results, figure 16 demonstrates that both charge measurements systems are in linear relation to one another, where the slope k is given by the geometry of both systems. Consequentially, after knowing k, values measured with the plate can be compared to values measured with the cup and vice versa - both systems can be used supplementary. The theory presented in 3.8 and 4.3 manages to explain some aspects of the discharging process due to pressure change but is insufficient in explaining all observations. First off, the model is capable of describing the quantitative trend of the discharging process as seen from the plate reading. Additionally, it gives two ways of calculating the amount of charge the sample still has after discharge, $Q_S(t_3)$. Even though d_{exp} and d_{th} do not exactly match, they follow the same trend (figure 21). Note that d_{exp} is the more correct version of d, since it explicitly takes a measurement at t_3 into account, while d_{th} extracts d purely from the measurement during discharge.

At the end of section 3.8.3, we shortly address the fact that the charge does not drop to zero upon Paschen discharge - an experimental fact shown in section 4.3. This could be due to the fact that the discharge process is dynamic - as soon as the magnitude of the electric field drops below the required value, discharge stops. The electric field could be insufficient after partial discharge because charges adsorb on the plate and the sample. As the adsorbed charges lower the total amount of charge on both objects, the electric field between them gets weaker. This explanation would imply that the remaining charge on the sample after Paschen discharge corresponds to a voltage $V < V_B$ - something that has not been experimentally confirmed here.

However, in addition to not fully discharging, another interesting phenomenon is sometimes observed. Figure 19b shows an example of a pump-down process where the discharge appears to occur in more than one step, something that is not directly addressed by the theoretical approach of the discharging process. A potential way of interpreting this process is given by the following. At constant distances between two probes, a tuple of two values for pressure and voltage (p,V) dictate a unique position in the Paschen diagram, hence a point in the (p, V) space. If the system now evolves in time where either p or V change, its evolution is represented by a line. At $t = 0$, we start with an initial value p_0 that is high compared to the Paschen minima as well as $V_0 > V_B$. Now p is gradually reduced. This process is illustrated in figure 28.
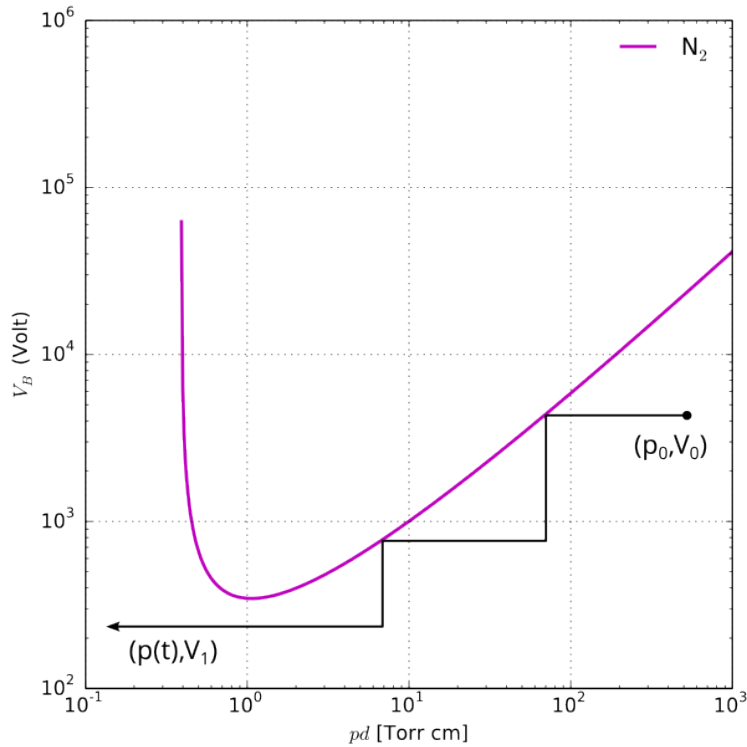
Figure 28: A schematic illustration showing how the process of multiple discharge events can be interpreted in a Paschen diagram. The black line represents the evolution of the system in the (p, V) space. Adapted from (12). License information given in appendix A.

As long as the black line remains below the Paschen curve, no discharge occurs, hence V remains unchanged. However, as soon as the black line intersects with the Paschen curve, discharge will occur, and V will drop to some extent. If, afterwards, V is still greater than $V_{min} = V(p_{min})$, the line can intersect with the Paschen curve again, leading to another discharging event. This can continue on until $V < V_{min}$, marking a voltage value insufficient of causing discharge, denoted as V_1 in figure 28. While this analysis might make the concept of multiple discharges more plausible, it naturally poses the question why the sample does not discharge all the way to $V \leq V_{min}$ on the first "contact" with the Paschen curve. In order to approach this, the microscopic mechanism of gas discharge would need to be revisited, perhaps with a dynamic model of the electric field between the samples, as mentioned above. This, however, is not attempted here.

Now the QMS measurement in figure 26 is shortly discussed. In this figure, the rate of ions starts out at zero, reaches a clear maximum as temperature keeps rising and drops back to a comparatively small value upon further temperature increase. Upon visual inspection, this appears to resemble a typical desorption curve. However, in order to be able to make more precise statements regarding various desorption parameters, more experimental data is necessary. E_{des} can for example be extracted from plotting $ln(r)$ over $\frac{1}{T}$ for many experiments, as explained in 2.3.2. This requires multiple repetitions of the same experiment at different temperatures and is

not done here. Additionally, different other molecules/atoms could have desorbed without being detected, since the QMS was only set to measure certain types of $\frac{m}{q}$ values. Masses close to the mass of water molecules (18 amu) have been chosen to investigate the possibility of water layers playing a role in the context of contact charge exchange as mentioned in section 2.1.2. The signals obtained with sample contacts at vacuum (figures 24 and 27) show a rate of almost zero ions at all times, therefore no desorption is observed. The reason for this, however, remains unclear. Perhaps the charge exchange mechanism itself is heavily pressure dependent, leading to different processes in different pressure regimes.

5.2. Outlook

If at some point reproducible desorption spectra are obtainable, the total amount of measured ions can be correlated to the exchanged charge given by the charge measurement system. This way, we could verify if the amount of desorbed ions actually scale with the total charge exchanged. If samples are homogeneously charged upon contact, multiple experiments with different total magnitudes of exchanged charge can form a plot, where the number of ions measured by the QMS is plotted against the Faraday cup signal. A sketch of such a plot is shown in figure 29.
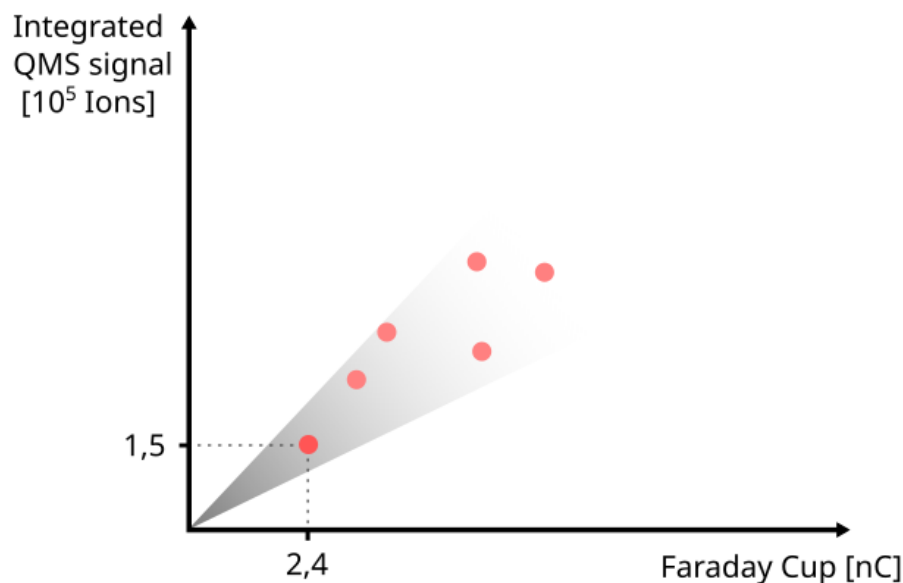
Figure 29: Schematic correlation between the amount of ions measured with the QMS and the charge picked up by the Faraday cup. The first dot corresponds to a measurement, the rest are for illustrative purposes only.

If all red dots in figure 29 approximately corresponded to a straight line, this would constitute strong evidence of ions taking the role of charge carriers in contact charging. However, this would only work in such a straight forward way if the samples

charge density is positive or negative on the whole surface. Some researches suggest that this might not always be the case. Instead they discuss the existence of charged patches, regions of positive Q_+ and negative Q_- charge distributed across the surface (3). In such a scenario, the total charge of a surface is given by $\Delta Q = Q_+ - Q_-$. Since the QMS can only measure Q_+ or Q_- but the Faraday structures measure ΔQ, these two quantities have no reason to be correlated, even if ionic charge exchange and desorption has occurred. Nevertheless, this problem can be avoided by using samples that are experimentally shown to only charge positive or negative with Kelvin probe force microscopy (KPFM), as specifically carried out by (41) for contact charging experiments between SiO_2 and PDMS.

There are still ways to improve the setup presented in this thesis such that certain phenomena can be studied in higher detail. In sections 4.3 and 2.2 the breakdown voltage V_B is discussed and put into context with experimental results. However, due to the lack of a precise pressure measurement, $p(t)$ and therefore $V(p)$ cannot be determined. An accurate pressure monitoring could be very helpful in understanding why samples only partially discharge and evaluate how accurate Paschen's law is in describing V_B. On the same note, evolutions in (p, V) space regarding discharging events with more than one step (such as the one shown in figure 28), could be checked experimentally. Additionally, a quick experiment that could potentially offer valuable insight into thermal desorption of ionic charge could go as follows. A sapphire sample could be charged up via contact, the amount of exchanged charge would be monitored with both charge measurement systems. The sapphire would then be heated up to sufficient temperatures while facing the QMS. Afterwards, the system relaxes back to room temperature and one would measure the remaining charge of the sapphire. If it was still charged to the exact same extent, thermal desorption of the charge carriers has likely not worked, regardless of the signal obtained by the QMS. On the other hand, if the sample was less charged than it was before, the picture of thermally desorbing ions remains an option.

6. Conclusion

Over the course of this project, a complex mass spectrometer experiment in the field of contact electrification is partially designed, developed and set up. As the cause for contact charge exchange with insulating materials is still unclear, electrons and ions are both plausible candidates as the charge carriers. In order to figure out the role of ions in contact charging, we put two samples inside a vacuum chamber where they can be brought into contact to exchange charge. Since charge measurements alone are usually insufficient to distinguish between electronic and ionic transfer, a QMS is utilized. If surface ions can be thermally desorbed, QMS measurements should be sufficient in determining whether ionic charge transfer plays a role in contact charging.

In order to be able to measure charge exchange, two different charge measurement systems, a Faraday plate and a Faraday cup, are designed and implemented. Both systems are then quantified and shown to work in alliance with one another. Charge exchange between two samples is analyzed at different pressure levels and compared regarding the usability for this experiment. It is shown that contact charging at atmospheric pressure results in a more reliable charge exchange than contacts at low pressure. Further on, the behaviour of charged surfaces under varying pressure is analyzed theoretically as well as experimentally. The interplay between Paschen's law, describing the breakdown voltage of gas, and electrostatic effects leads to a compact way of interpreting signals obtained with a Faraday plate. An experimental comparison shows that the theoretical framework is successful in explaining various key aspects of the observed data. Moreover, preliminary QMS desorption spectra show that thermal desorption of ions appears to be possible, however more experimental data is required to make preciser statements. Finally, due to the efforts presented in this thesis, this setup is now considerably closer towards potentially uncovering the role of ions within the triboelectric effect.

References

[1] D. J. Lacks and R. M. Sankaran, "Contact electrification of insulating materials," *Journal of Physics D: Applied Physics*, vol. 44, no. 45, p. 453001, October 2011. [Online]. Available: https://doi.org/10.1088/0022-3727/44/45/453001

[2] C. Kittel, *Introduction to Solid State Physics*, 9th ed., 2018, no. ISBN 978-1-119-45416-8.

[3] D. J. Lacks and T. Shinbrot, "Long-standing and unresolved issues in triboelectric charging," *Nature Reviews Chemistry*, pp. 465 – 476, August 2019. [Online]. Available: https://doi.org/10.1038/s41570-019-0115-1

[4] F. Paschen, "Ueber die zum funkenübergang in luft, wasserstoff und kohlensäure bei verschiedenen drucken erforderliche potentialdifferenz," *Annalen der Physik*, vol. 273, no. 5, pp. 69–96, 1889. [Online]. Available: https://onlinelibrary.wiley.com/doi/abs/10.1002/andp.18892730505

[5] G. Grosjean, S. Wald, J. C. Sobarzo, and S. Waitukaitis, "Quantitatively consistent scale-spanning model for same-material tribocharging," *Phys. Rev. Materials*, vol. 4, p. 082602, August 2020. [Online]. Available: https://link.aps.org/doi/10.1103/PhysRevMaterials.4.082602

[6] N. W. Ashcroft and N. D. Mermin, *Solid State Physics*. Holt-Saunders, 1976.

[7] J. Lowell and W. S. Truscott, "Triboelectrification of identical insulators. ii. theory and further experiments," *Journal of Physics D: Applied Physics*, vol. 19, no. 7, p. 1281, jul 1986. [Online]. Available: https://dx.doi.org/10.1088/0022-3727/19/7/018

[8] J. Wilcke, *Disputatio physica experimentalis, de electricitatibus contrariis ...* Typis Ioannis Iacobi Adleri, 1757. [Online]. Available: https://books.google.at/books?id=Mld_nQEACAAJ

[9] P. E. Shaw, "The electrification of surfaces as affected by heat," *Proceedings of the Physical Society of London*, vol. 27, no. 1, p. 208, dec 1914. [Online]. Available: https://dx.doi.org/10.1088/1478-7814/27/1/317

[10] A. Seaver, "Tribocharging and the finite thickness interface," *Proc. Jt. Electrost. Conf.*, 01 2012.

[11] E. Husain and R. S. Nema, "Analysis of paschen curves for air, n2 and sf6 using the townsend breakdown equation," *IEEE Transactions on Electrical Insulation*, vol. EI-17, no. 4, pp. 350–353, 1982.

[12] Krishnavedala, "Paschen curves," 2014, [accessed January 15, 2024]. [Online]. Available: https://commons.wikimedia.org/wiki/File:Paschen_curves.svg

[13] K. Oura, M. Katayama, A. V. Zotov, V. G. Lifshits, and A. A. Saranin, *Surface Science - An Introduction*. Springer, April 3, 2004.

[14] A. Zangwill, *Physics at Surfaces*, 1988, no. ISBN 978-0-521-34752-5.

55

[15] porphyrin, "How does adsorption work?" 2016, [accessed January 20, 2024]. [Online]. Available: https://chemistry.stackexchange.com/questions/54576/is-the-rate-of-desorption-dependent-on-pressure/54579#54579

[16] R. L. Baumann, J. L. Falconer, and N. Bongiardina, "Temperature-programmed desorption," 2013, [accessed February 25, 2024]. [Online]. Available: https://demonstrations.wolfram.com/TemperatureProgrammedDesorption/

[17] P. Redhead, "Thermal desorption of gases," vol. 12, no. 4, pp. 203–211, 1962.

[18] R. A. Alberty and R. J. Silbey, *Physical chemistry*. John Wiley & Sons, Inc., June 2004. [Online]. Available: https://www.wiley.com/en-hk/Physical+Chemistry%2C+4th+Edition-p-9780471215042

[19] D. G. Bills, "Ion desorption from metal surfaces," *Phys. Rev.*, vol. 107, pp. 994–995, Aug 1957. [Online]. Available: https://link.aps.org/doi/10.1103/PhysRev.107.994

[20] A. Riddoch and J. H. Leck, "Positive ion emission from metal surfaces caused by ion bombardment," *Proceedings of the Physical Society*, vol. 72, no. 3, p. 467, sep 1958. [Online]. Available: https://dx.doi.org/10.1088/0370-1328/72/3/422

[21] M. L. Knotek, "Study of the thermal desorption of ions from the surface of β-alumina," *Phys. Rev. B*, vol. 14, pp. 3406–3414, Oct 1976. [Online]. Available: https://link.aps.org/doi/10.1103/PhysRevB.14.3406

[22] H. ANALYTICAL, *IDP Analyser User Manual*, HIDEN.

[23] S. E. V. Bramer, "An introduction to mass spectrometry," *Widener University, Department of Chemistry*, September 1998. [Online]. Available: https://science.widener.edu/svb/massspec/massspec.pdf

[24] J. W. Honour, "Benchtop mass spectrometry in clinical biochemistry," *Annals of clinical biochemistry*, vol. 40, pp. 628–38, 12 2003.

[25] R. E. March, "An introduction to quadrupole ion trap mass spectrometry," *Journal of Mass Spectrometry*, vol. 32, pp. 351–369, 1997. [Online]. Available: https://api.semanticscholar.org/CorpusID:16506573

[26] W. Demtröder, *Experimentalphysik 3 - Atome, Moleküle und Festkörper*, 5th ed. Springer, 2016, no. 978-3-662-49093-8.

[27] M. S. PRO, "Electron multiplier," 2023, [accessed January 15, 2024]. [Online]. Available: http://www.massspecpro.com/detectors/electron-multiplier

[28] Thorlabs, "Sapphire windows," 2023, [accessed November 23, 2023]. [Online]. Available: https://www.thorlabs.com/newgrouppage9.cfm?objectgroup_id=3982&pn=WG31050

[29] Roditi, "Sapphire properties 1," 2023, [accessed November 28, 2023]. [Online]. Available: https://www.roditi.com/SingleCrystal/Sapphire/Properties.html

[30] G. O. Associates, "Sapphire properties 2," 2023, [accessed November 28, 2023]. [Online]. Available: https://www.guildoptics.com/sapphire-properties/sapphire-properties/

[31] M. S. PRO, "The pid controller & theory explained," 2023, [accessed January 16, 2024]. [Online]. Available: https://www.ni.com/en/shop/labview/pid-theory-explained.html

[32] K. A. T. Company, *Model 6514 System Electrometer Instruction Manual*, KEITHLEY.

[33] K. A. T. company, *Keithley Low Level Measurements Handbook - 7th Edition*, KEITHLEY.

[34] J. Kindersberger and C. Lederle, "Surface charge decay on insulators in air and sulfurhexafluorid – part i: Simulation," *IEEE Transactions on Dielectrics and Electrical Insulation*, vol. 15, no. 4, August 2008.

[35] SIMCOION, "Frequently asked questions - how does air ionization work?" 2024, [accessed February 19, 2024]. [Online]. Available: https://technology-ionization.simco-ion.com/resources/faqs

[36] A. Zangwill, *Modern Electrodynamics*, 2013, no. ISBN 978-0-521-89697-9.

[37] HAMAMATSU, *PhotoIonizer L12645 Instruction Manual*, HAMAMATSU.

[38] H. P. K. K., "Principle of operation," 2022, [accessed April 18, 2022]. [Online]. Available: https://www.hamamatsu.com/us/en/product/manufacturing-support-systems/electrostatic-remover/electrostatic-remover/L12645.html

[39] G. Grosjean and S. Waitukaitis, "Single-collision statistics reveal a global mechanism driven by sample history for contact electrification in granular media," *Phys. Rev. Lett.*, vol. 130, p. 098202, Feb 2023. [Online]. Available: https://link.aps.org/doi/10.1103/PhysRevLett.130.098202

[40] I. I. D. S. GmbH, "Ids camera," 2023, [accessed November 30, 2023]. [Online]. Available: https://en.ids-imaging.com/download-details/AB.0010.1.28000.00.html

[41] F. Pertl, J. C. Sobarzo, L. Shafeek, T. Cramer, and S. Waitukaitis, "Quantifying nanoscale charge density features of contact-charged surfaces with an fem/kpfm-hybrid approach," *Phys. Rev. Mater.*, vol. 6, p. 125605, Dec 2022. [Online]. Available: https://link.aps.org/doi/10.1103/PhysRevMaterials.6.125605

List of Figures

A. Licensing

- Figure 3

  This figure is published under the following license: CC BY-SA 4.0 Deed. Link: `https://creativecommons.org/licenses/by-sa/4.0/`

- Figure 5

  This material is published under the following license: CC BY-NC-SA 3.0 Deed. Link: `https://creativecommons.org/licenses/by-nc-sa/3.0/`

- Figure 6

  DOI: `https://doi.org/10.1103/PhysRevB.14.3406`, License:

APS American Physical Society
Reuse and Permissions License

06-Apr-2024

This license agreement between the American Physical Society ("APS") and Markus Felber ("You") consists of your license details and the terms and conditions provided by the American Physical Society and SciPris.

Licensed Content Information

License Number:	**RNP/24/APR/077756**
License date:	06-Apr-2024
DOI:	10.1103/PhysRevB.14.3406
Title:	Study of the thermal desorption of ions from the surface of b-alumina
Author:	M. L. Knotek
Publication:	Physical Review B
Publisher:	American Physical Society
Cost:	USD $ 0.00

Request Details

Does your reuse require significant modifications:	No
Specify intended distribution locations:	Worldwide
Reuse Category:	Reuse in a thesis/dissertation
Requestor Type:	Student
Items for Reuse:	Figures/Tables
Number of Figure/Tables:	1
Figure/Tables Details:	thermal desorption curves of Potassium
Format for Reuse:	Print
Total number of print copies:	Up to 1000

Information about New Publication:

University/Publisher:	TU WIEN
Title of dissertation/thesis:	Towards Uncovering the Charge Carriers in Tribocharging
Author(s):	Markus Felber
Expected completion date:	Apr. 2024

License Requestor Information

Name:	Markus Felber
Affiliation:	Individual
Email Id:	markus.felber@tuwien.ac.at
Country:	Austria

- Figure 28

  This figure is published under the following license: CC BY-SA 4.0 Deed. Link: `https://creativecommons.org/licenses/by-sa/4.0/`